

NASA Contractor Report 178046

SUBSONIC FLOW INVESTIGATIONS ON A CRANKED WING
DESIGNED FOR HIGH MANEUVERABILITY

Dhanvada M. Rao

(NASA-CR-178046) SUBSONIC FLOW
INVESTIGATIONS ON A CRANKED WING DESIGNED
FOR HIGH MANEUVERABILITY Final Report
(Vigyan Research Associates, Inc.) 45 p
HC A03/MF A01

N86-20361

Unclas
05686

CSCL 01A G3/02

VIGYAN RESEARCH ASSOCIATES, INC.
Hampton, Virginia 23666

Contract NAS1-17420
February 1986

NASA
National Aeronautics and
Space Administration
Langley Research Center
Hampton, Virginia 23665



TABLE OF CONTENTS

	<u>Page</u>
INTRODUCTION	1
LIST OF SYMBOLS	1
EXPERIMENTAL DETAILS	2
BASIC WING CHARACTERISTICS	2
TIP PANEL FLOW CONTROL CONCEPTS	5
RESULTS OF FLOW CONTROL CONCEPTS	6
N.C.S.U. SEMI-SPAN MODEL:	6
Fence	6
Pylon Vortex Generator	7
Mid-Span Strake	7
Cavity Flap	8
LRC WING/BODY MODEL:	8
THEORETICAL PREDICTION OF BASIC WING FORCE CHARACTERISTICS	9
CONCLUSIONS AND RECOMMENDATIONS	10
ACKNOWLEDGEMENT	11
REFERENCES	11

INTRODUCTION

This report summarizes the main results of exploratory experiments on flow control devices applied to a cranked-wing planform, with the object of increasing the subsonic maneuverability of supersonic fighter designs under evaluation in the NASA Langley Advanced Concepts Branch, HSAD. The first part of the study was devoted to understanding the basic flow phenomena responsible for usable lift limitation on an uncambered 70 deg./50 deg. cranked wing, due to onset of pitching moment non-linearity and longitudinal instability. With the insight gained into flow separation phenomenon and the formation and growth of vortices with increasing angle of attack, several flow control device concepts were proposed for improving the cranked wing pitch characteristics in order to increase the usable C_L . The prospects and limitations of these concepts were explored, and recommendations made for further research.

LIST OF SYMBOLS

C	Local chord
C_D	Drag coefficient
C_{D0}	Zero-lift drag coefficient
C_L	Lift coefficient
C_m	Pitching moment coefficient
C_N	Normal force coefficient
C_p	Pressure coefficient
$C_{p,U}$	Upper-surface pressure coefficient
H.L.	Hinge line station
PVG	Pylon vortex generator
x	Chordwise distance from leading edge (positive upper surface, negative lower surface)

α	Angle of attack
ϵ	Upwash angle
η	Spanwise distance as fraction of wing semi-span
ϕ	Sidewash angle

EXPERIMENTAL DETAILS

Two separate wind tunnel investigations were conducted. A semi-span wing model of composite construction, incorporating upper-surface static pressure taps along two chordwise rows was tested in the North Carolina State University 32 inch x 45 inch subsonic tunnel. This model was also used for extensive flow visualizations. The major dimensions of this model and its vertical mounting on a reflection plane are shown in fig. 1. The pressure and oil-flow tests were conducted at a nominal free-stream velocity of 90 ft/sec., corresponding to a mean-chord Reynolds number of 0.9×10^6 . For helium-bubble visualizations the test speed was approximately 20 ft/sec.

The balance model in the form of a wing/body configuration, tested in the NASA Langley 12-ft Low Speed Tunnel, is shown in fig. 2. The tests were run at a free-stream velocity of 70 ft/sec. giving a mean-chord Reynolds number of 0.92×10^6 .

The geometry and major dimensions of the flow control devices as tested on the NCSU semi-span model are shown in fig. 3. The fence and pylon vortex generators on the Langley force model were scaled with respect to the wing chord at the crank.

BASIC WING CHARACTERISTICS

To help understand its low-speed aerodynamics characteristics, the cranked wing may be viewed as a conventionally swept wing having a relatively large apex

extension (or strake). The conventionally-swept wing stalls in the tip region, where a combination of high aerodynamic loading and boundary layer build-up leads to early separation. The thin wing sections near the tip rapidly develop leading-edge flow separation covering the full chord length, producing marked lift loss and drag rise.

The addition of a highly swept apex region generates a pair of counter-rotating leading edge vortices, which persist downstream to the wing trailing edge. These apex vortices are stabilized by flow reattachment to the wing surface. A high suction level induced on the wing underneath each vortex core generates additional lift, which rapidly increases with angle of attack. Furthermore, the rotational field of the vortex induces a sidewash component directed towards the tips, which increases the effective sweep angle of outboard leading edges. Thus, an outboard leading edge vortex originates from the crank, which serves to stabilize the flow separation and generates vortex lift on the outer panel.

The apex vortex also induces a vertical velocity on the crank vortex, tending to raise it away from the outer panel surface. When at some angle of attack the apex vortex has gained considerable strength, it rapidly displaces the crank vortex upwards as depicted in fig. 4, resulting in a pronounced loss of outer-panel lift. Increasing angle of attack also moves the breakdown position of the apex vortex in the wake towards the trailing edge. Progression of the vortex breakdown forward over the wing surface reduces the vortex lift on the inboard regions of the wing.

The upper-surface flow visualizations and pressure measurements on the basic cranked wing broadly confirm the flow development pictured above. A sequence of oil-flow photographs at increasing angle of attack is presented in fig. 5. The upper-surface flow at $\alpha = 5$ deg. is fully attached. At $\alpha = 10$

and 15 deg. the characteristic tracks produced by the apex and crank vortices on the wing surface are separate and traceable back to the trailing edge. At $\alpha = 17$ deg. however, the crank-vortex track abruptly disappears well ahead of the trailing edge, and the spanwise boundary layer flow penetrates farther into the outer panel. A second sequence of oil-flow photographs shown in fig. 6 shows the crank-vortex track continuing to shrink with further increase in angle of attack.

A series of helium bubble visualizations is presented in fig. 7. Each picture is a composite of two separate photographs, obtained with the bubble-generator moved from the apex to the crank position for better definition of the respective vortices. At $\alpha = 15$ deg. the two vortex cores remain distinct. At higher angles of attack, massive flow separation on the outer panel defeated attempts to get the bubbles closer to the wing surface, and the crank vortex could only be glimpsed occasionally. The apex vortex core however remained easily identifiable; the onset and progress of its breakdown is seen in the photographs for $\alpha = 25$ deg. and 30 deg. (A video-tape record of the helium bubble visualization tests can be obtained from ViRA, Inc.)

Chordwise pressure distributions at the inboard and outboard stations with increasing angles of attack are presented in fig. 8. The upper-surface flow remains attached at $\alpha = 5$ deg., but $\alpha = 10$ deg. local suction peaks reveal the presence of apex and crank vortices at the respective stations. The inboard suction peak continues to develop with increasing angle of attack, but the outboard pressure distributions rapidly flatten out indicating full-chord separation starting at $\alpha = 15$ deg.

The local normal force coefficients, obtained by integrating the above pressure distributions, are plotted versus angle of attack in fig. 9. This comparison highlights the load trends above $\alpha = 10$ deg., at which point the

outboard panel stalls while the inboard section continues to generate strong vortex lift. Consequently a progressive longitudinal instability would be anticipated above $\alpha = 10$ deg.

The lift and pitching moment measurements (on the wing-body model of fig. 2) are shown in fig. 10. The moment data confirm the expected longitudinal instability onset at $\alpha = 10$ deg.; however the lift-curve slope remains continuous across $\alpha = 10$ deg. implying that the growth of vortex lift over the inboard region is compensating for the decreasing lift on the outboard panel. These results serve to emphasize the large disparity between usable and available maximum lift coefficients typical of a crank wing, and indicate considerable potential for improving its maneuver and low-speed capability through effective control of the outer panel flow at high angles of attack.

TIP PANEL FLOW CONTROL CONCEPTS

The effectiveness of conventional leading-edge deflection to prevent outer panel stall on this wing would appear to be constrained by excessive upwash induced locally, e.g. the chord-plane flow angle exceeding 50 deg. at $\alpha = 20$ deg. as indicated by potential flow calculations (using PAN AIR code) presented in fig. 11,A. At such high deflections of a leading edge flap, severe hinge-line flow separation may be expected which largely cancels the advantage of achieving a smooth on-flow. This problem may be avoided by the use of vortex flaps; however the typically large tip chord of such flaps poses structural and actuation problems. While a leading edge flap offers the advantage of drag reduction, other concepts than those relying on camber variation for outer-panel flow control appeared worth considering.

In the present study, three alternative schemes were conceived as depicted in fig. 12 and explained below:

- A). Generate a control vortex at the crank, opposite in rotation to the leading-edge vortices. The purpose of this vortex would be to induce a downward velocity on the crank vortex resisting its lift-off tendency. The fence and pylon vortex generator are two different means of creating this control vortex, and may be employed in combination.
- B). Generate a control vortex near the crank having the same rotational sense as the leading edge vortex. This new vortex would serve to energize the stalling flow on the tip panel, much as a wing-root strake. A relatively small folding strake that can be deployed at a specified angle of attack is envisaged.
- C). A lower-surface hinged flap to trap a vortex just below the leading edge. This spanwise vortex serves the dual purpose of (a) assisting the incident flow at high upwash angle to turn towards the outer wing panel surface, and (b) moderating the intensity of vortex lift generated on the inner wing and thus reducing the unstable pitching moment. The vortex suction induced in the 'cavity' produces a vortex-flap type of thrust component for the additional benefit of drag reduction.

RESULTS OF FLOW CONTROL CONCEPTS

N.C.S.U. SEMI-SPAN MODEL:

Fence - The effect of a chordwise fence on the outboard upper-surface pressure distribution at several angles of attack is shown in fig. 13. In comparison with the basic wing, the fence generates higher levels of suction

over the outboard panel. While this suction increment gradually diminishes with increasing angle of attack, an opposite effect occurs between $\alpha = 25$ deg. and 30 deg. In the corresponding oil flow visualizations presented in fig. 14, a rapid growth of the fence vortex can be inferred especially at $\alpha = 20$ deg. and 25 deg. Apparently the fence vortex is further intensified at $\alpha = 30$ deg., when its spanwise influence extends to the whole of the tip region.

Pylon Vortex Generator - The effects produced by a crank-located PVG are shown in fig. 15. A distinct suction peak at $\alpha = 15$ deg. suggests the persistence of a crank vortex, in contrast to the nearly uniform pressure on basic wing data. At higher angles of attack, the overall suction level increases relative to the basic wing. The pressure-integrated local normal force with PVG is compared with the basic wing in fig. 16. Included are results with the fence, and also a fence-PVG combination. Both these devices individually provide a 2 to 3 deg. increment in the angle of attack before reaching C_{Nmax} ; the rate of decline of the local normal force after C_{Nmax} is also moderated. In combination the improvement is even greater. These trends are distinctly favorable to pitch-up alleviation.

Mid-Span Strake - The outboard pressure distributions on the wing with an in-plane strake are presented in fig. 17. At all the test angles of attack a well-established vortex originating from the outboard junction of the strake and wing leading edge is indicated. A typical oil flow pattern at $\alpha = 20$ deg. presented in fig. 18 reveals the track of this vortex, and demonstrates the beneficial effect of the strake on the tip flow in comparison with the basic wing. Note also the considerable vortex action on the strake itself. The direct vortex lift on the strake being close to the wing centroid should not greatly influence the center of pressure. No overall force and moment data have yet been obtained for this configuration.

Cavity Flap - A preliminary test was performed with a 10- deg. deflected cavity flap attached under the outboard leading edge. The lower surface pressure at one location underneath the leading edge (i.e. in the flap cavity region) is plotted versus angle of attack in fig. 19. With the flap on, a negative pressure (relative to the basic wing) starts at $\alpha = 10$ deg., implying the onset of a cavity vortex. Thereafter, the cavity suction steadily increases with angle of attack. Spanwise exploration with a static pressure probe along the cavity corner revealed the suction level to be relatively uniform (fig. 20). The chordwise upper surface pressure distributions with the cavity flap on the outer panel (fig. 21) are not particularly informative, although the presence of a crank-vortex suction peak at $\alpha = 15$ deg. (in comparison with the flap-off case) suggests that a reduction of the local incidence might have occurred.

Results with a 30 deg. deflected cavity flap attached to the inboard (70 deg. swept) leading edge, are presented in fig. 22. In this case the upper-surface distributions clearly reveal a diminished primary vortex suction peak relative to the basic wing. The associated reduction of the nose-up moment on this section will help to improve longitudinal stability of the cranked wing. A pronounced suction generated in the flap cavity also is noted.* On the basis of these pressure results, force tests to evaluate the potential of cavity flaps for usable-lift enhancement as well as for drag reduction appear worthwhile.

LRC WING/BODY MODEL:

The main purpose of this test was to assess the fence and PVG devices in extending the longitudinally-stable C_L range of the cranked wing. The pitching moment characteristics with and without the devices are compared in fig. 23.

*Note: The capture of a stable cavity vortex was confirmed in water tunnel experiments performed cooperatively with Northrop Aircraft Corporation; a video-tape is available with ViRA, Inc.

An evaluation in terms of the stability derivative dC_m/dC_L of the devices is presented separately in fig. 24 and 25. Both the fence and the PVG clearly eliminate the basic wing pitch-up at $C_L = 0.65$ ($\alpha = 15$ deg.) The fence however is progressively destabilizing above $C_L = 0.4$, an effect not found with the PVG. In either case, the longitudinally stable limit of C_L is raised from 0.65 to 0.8. A strong pitch up noted just above $C_L = 0.8$ with the PVG could possibly be alleviated by the use of a second PVG located on the inboard leading edge, based on author's previous experience with multiple PVGs on delta wings (ref. 1).

THEORETICAL PREDICTION OF BASIC WING FORCE CHARACTERISTICS

The vortex lattice method incorporating the Polhamus suction analogy, or VLM-SA (ref. 2) has been generally successful in predicting the lift and drag characteristics of highly swept delta and strake-wing planforms with fully developed leading-edge vortices. The available options in VLM-SA are as follows (see fig. 26)

(L.E.S. = Leading Edge Suction)

<u>Option</u>	<u>Inboard L.E.</u>	<u>Outboard L.E.</u>
A	Vortex	Vortex
B	Vortex	Attached (full L.E.S.)
C	Vortex	"Separated" (zero L.E.S.)*
D	Attached (full L.E.S.)	Attached (full L.E.S.)
E	"Separated" (zero L.E.S.)*	"Separated" (zero L.E.S.)*

* This is a fictitious flow model, assumed to represent a fully-stalled condition.

In applying the VLM-SA method to the present cranked wing, a two-planform model was adopted: (I) the apex extension and, (II) the rest of the wing. (See sketch in fig. 27.) The 'augmented lift' concept was applied at the crank position to account for the induced lift of the shed apex vortex.

The lift characteristics predicted by the various VLM-SA options are compared with wind tunnel data in fig. 27. Even before vortex breakdown, the experimental lift capability of this wing is seen to fall considerably short of the full vortex lift prediction. Indeed, the best lift prediction (up to vortex breakdown) is obtained with the VLM-SA option C, i.e. assume full vortex lift on the inboard leading edge and zero vortex lift outboard. This is also true of the drag polar prediction, as shown in fig. 28. These calculations provide an indication of the attainable performance if full vortex lift could be sustained on the outboard leading edge at higher angles of attack.

CONCLUSIONS AND RECOMMENDATIONS

Exploratory flow visualizations and pressure tests were performed on a 70 deg./50 deg. cranked wing model to assess the potential of device concepts in controlling the tip-panel stall, in order to alleviate or postpone the onset of longitudinal instability to a higher lift coefficient. The concepts studied were (1) fence, (2) pylon vortex generator, (3) a folding strake and (4) cavity flap. The fence and PVG were also tested on a balance model.

Both the fence and PVG, individually and in combination, produced distinct and favorable effects on the vortex flow development and local normal-force characteristics on the tip panel, resulting in a C_L increment of 0.15 before instability onset. Refinement of the design and placement of these devices is expected to yield additional improvements.

Although the scale of these experiments was relatively small, the results are believed to be basically valid for full-scale Reynolds number, because the crank wing pitch-up problem as well as the proposed concepts for its alleviation involve sharp edge separation vortices and therefore should be only weakly Reynolds number dependent.

The limited but promising pressure and flow visualization results on the folding strake concept warrant balance testing in order to establish its lift-improvement potential.

Similarly, pressure measurements and flow visualization studies of the cavity flap concept were encouraging and a force test program is recommended.

ACKNOWLEDGEMENT

The assistance of Robert Vess, North Carolina State University, and Gregory Riebe, Advanced Concepts Branch (HSAD), NASA Langley, during the wind tunnel tests reported here is thankfully acknowledged.

REFERENCES

1. Rao, D. M. and Johnson, T. D., Jr.; "Alleviation of the Subsonic Pitch-Up of Delta Wings", J. Aircraft, Vol. 20, No. 6, June 1983, pp. 530-535.
2. Lamar, J. E.; "Summary of Some Recent Studies of Subsonic Vortex Lift and Parameters Affecting the Leading-Edge Vortex Stability", AIAA Paper 76-414, July 1974.

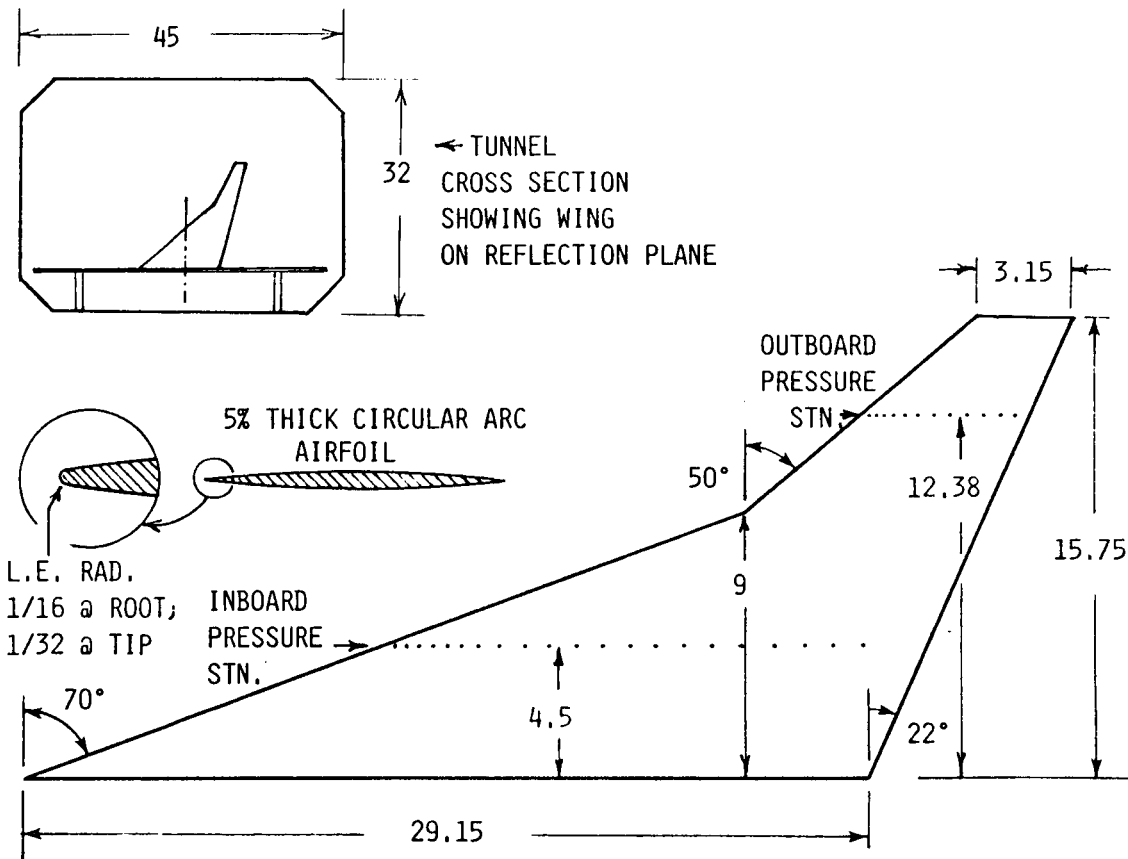


Figure 1 - Semi-span Wing Model tested in N.C.S.U. subsonic wind tunnel (dimensions in inches)

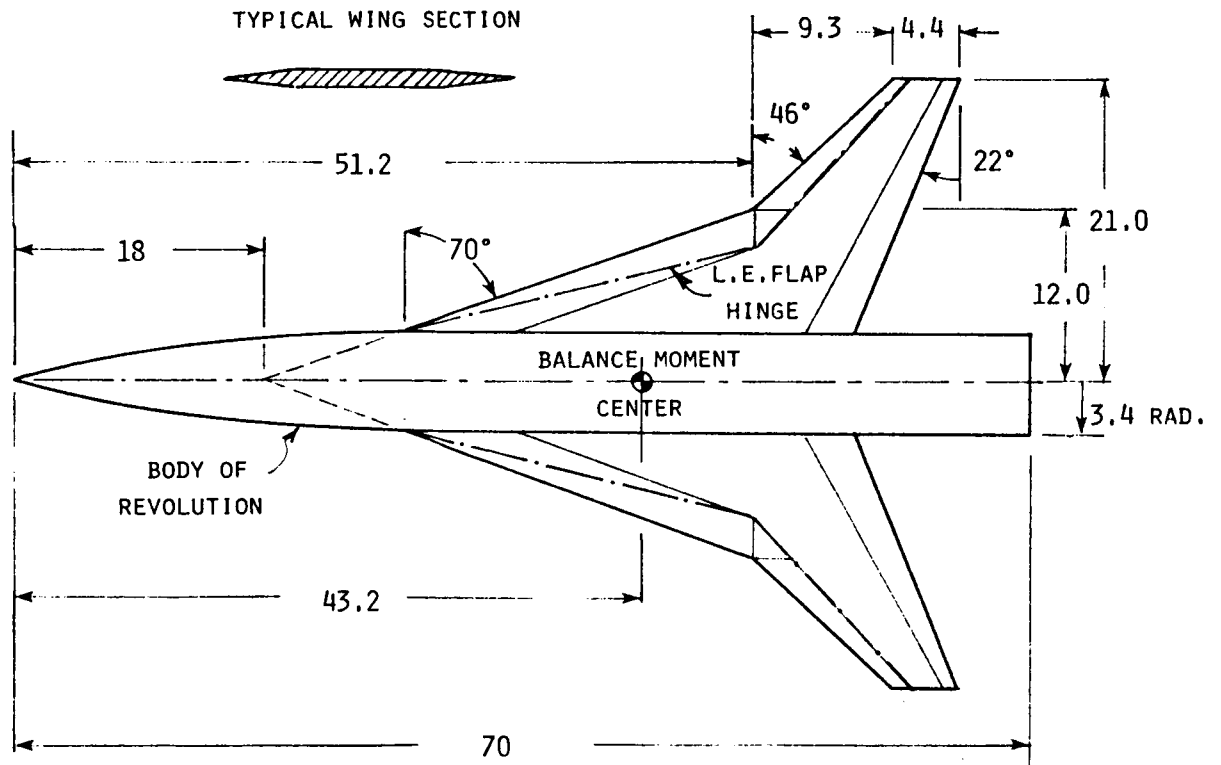
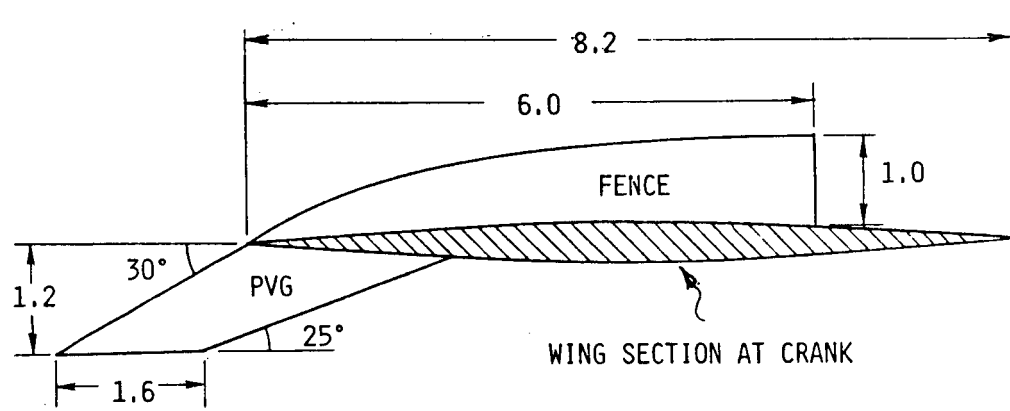
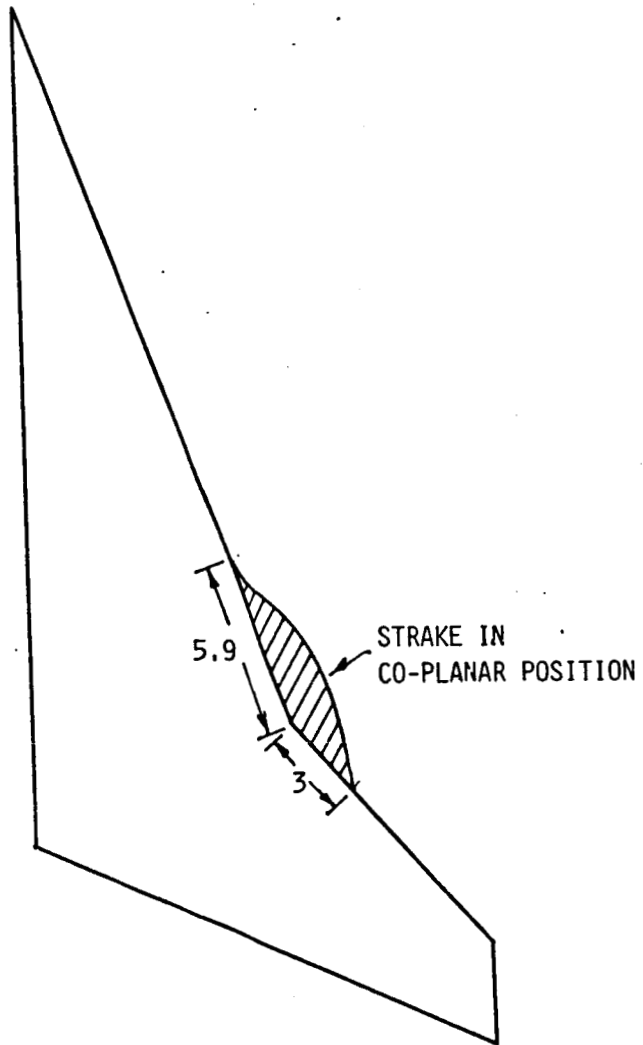


Figure 2 - Wing-body balance model tested in NASA Langley 12-ft low speed tunnel (dimensions in inches)



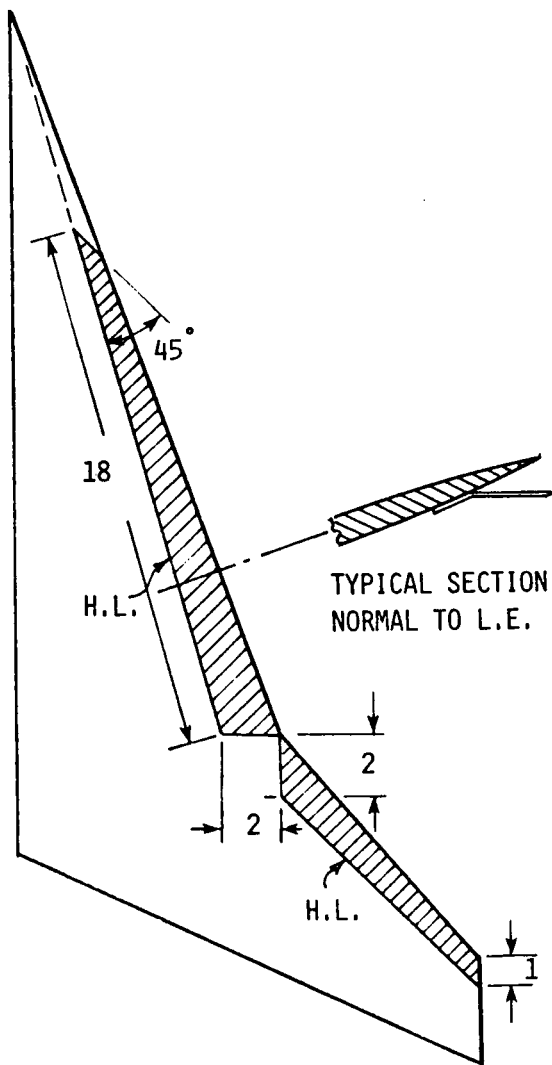
A) Fence and Pylon Vortex Generator

Figure 3 - Flow control devices (dimensions in inches)



B) Folding Mid-Span Strake

Figure 3 - Continued



C) Leading Edge Cavity Flap

Figure 3 - Concluded

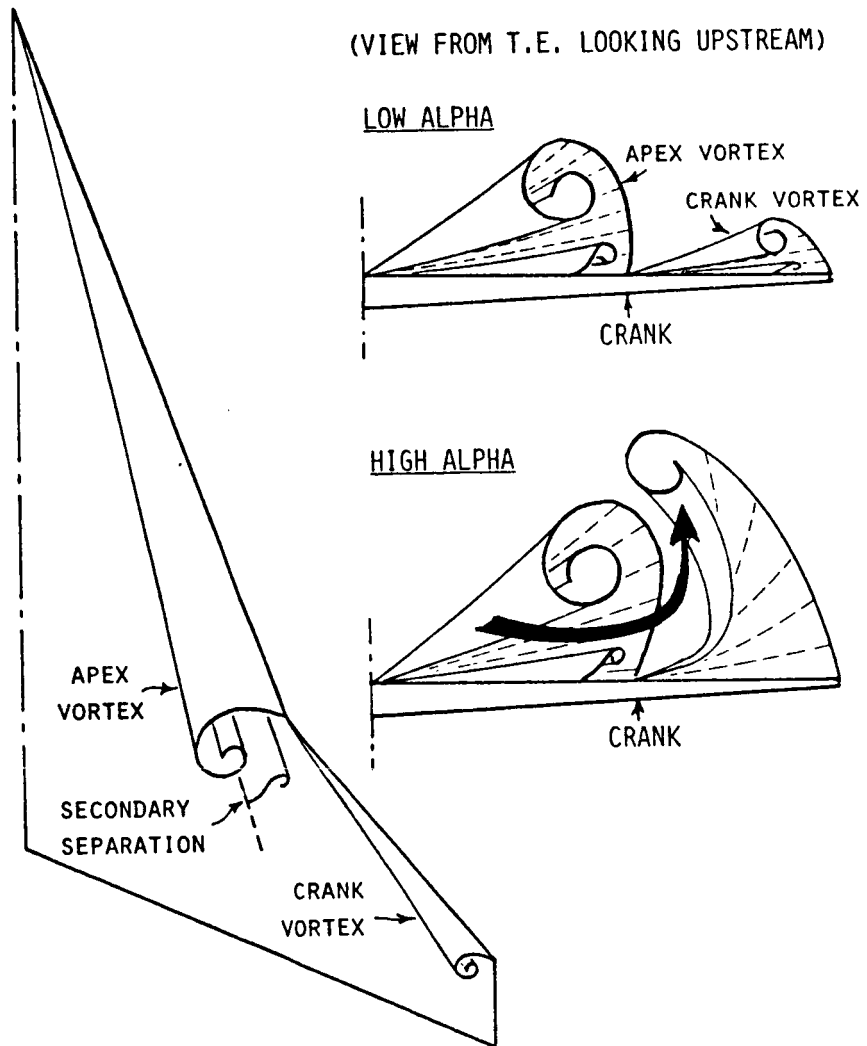


Figure 4 - Hypothesized development of leading edge vortices on cranked wing.

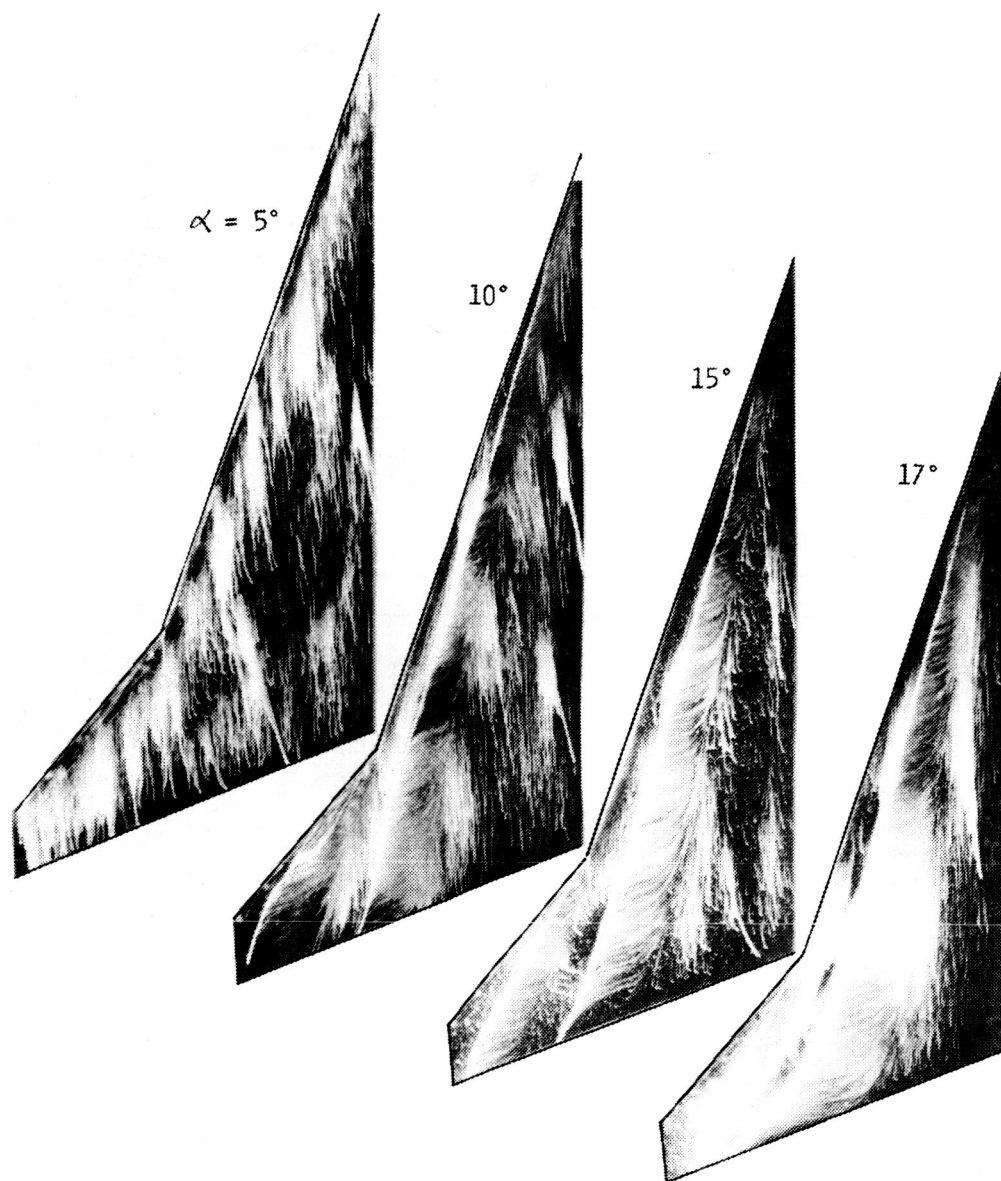


Figure 5 - Oil flow visualizations of basic cranked wing showing progression of tip panel stall ($\alpha = 5^\circ$ to 17°)

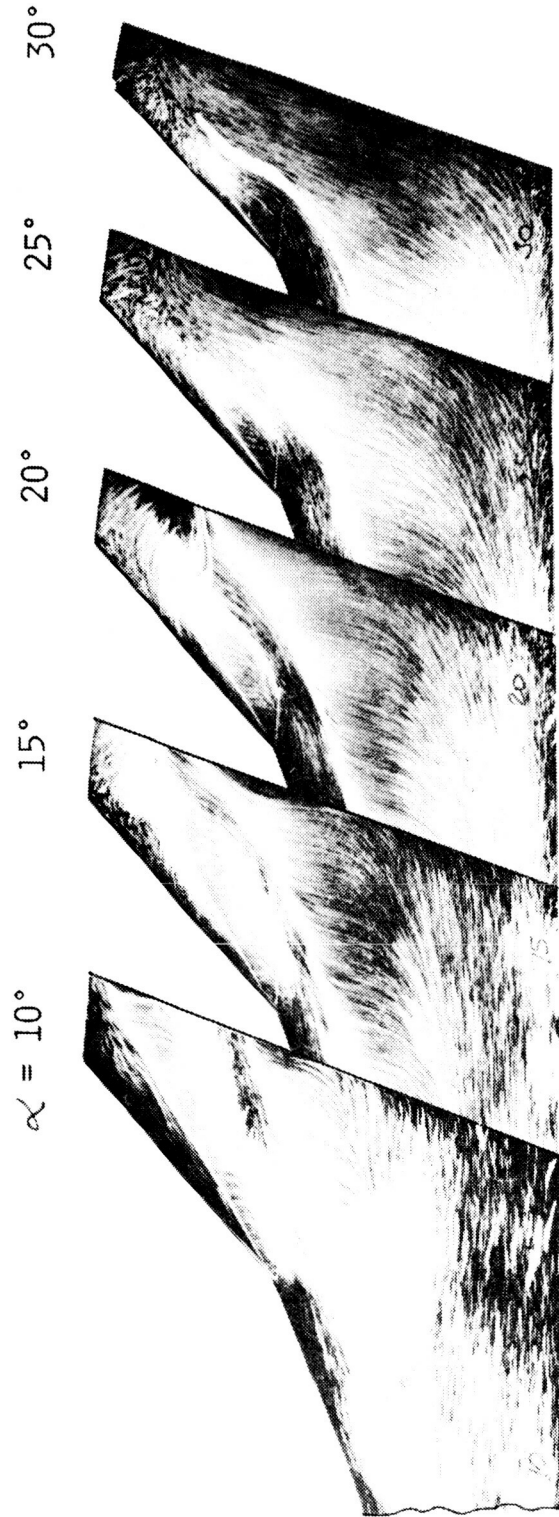


Figure 6 - Oil flow visualizations of basic wing showing progression of tip panel stall ($\alpha = 10^\circ$ to 30°)

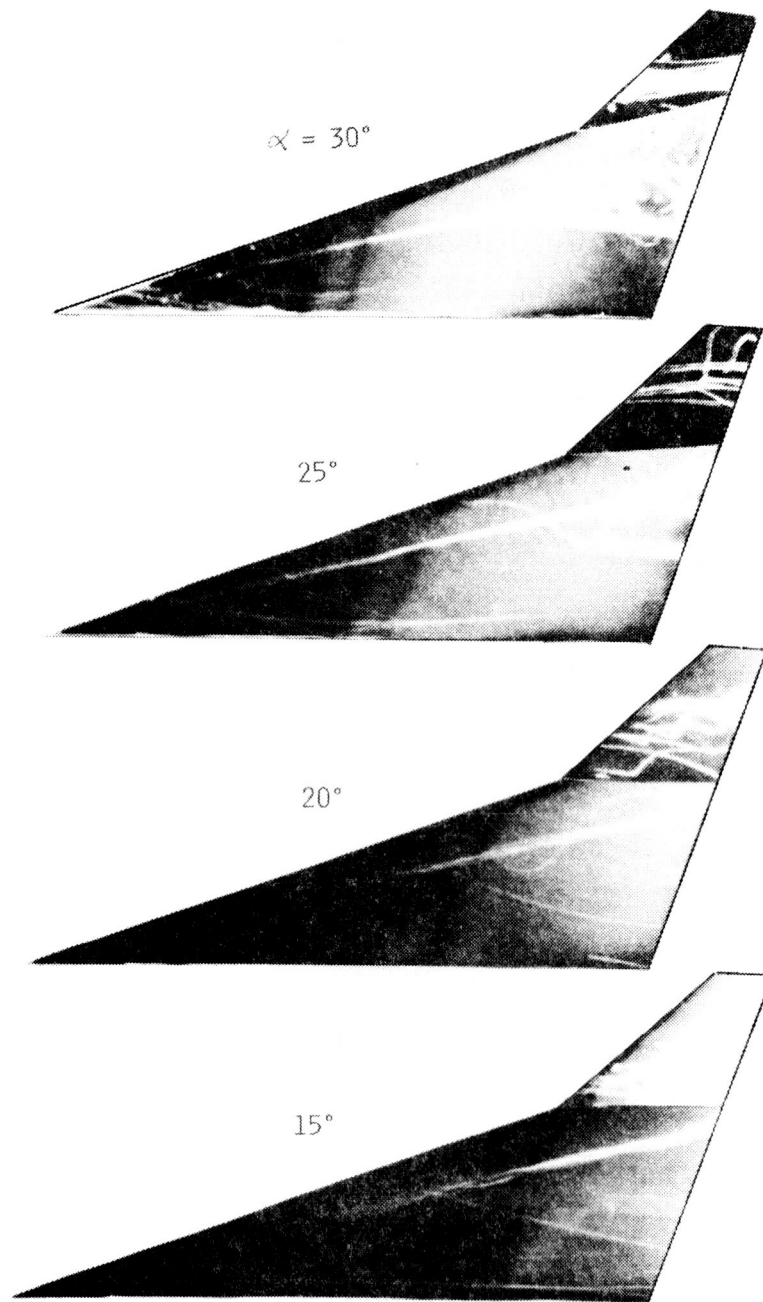


Figure 7 - Helium bubble visualizations of basic cranked wing

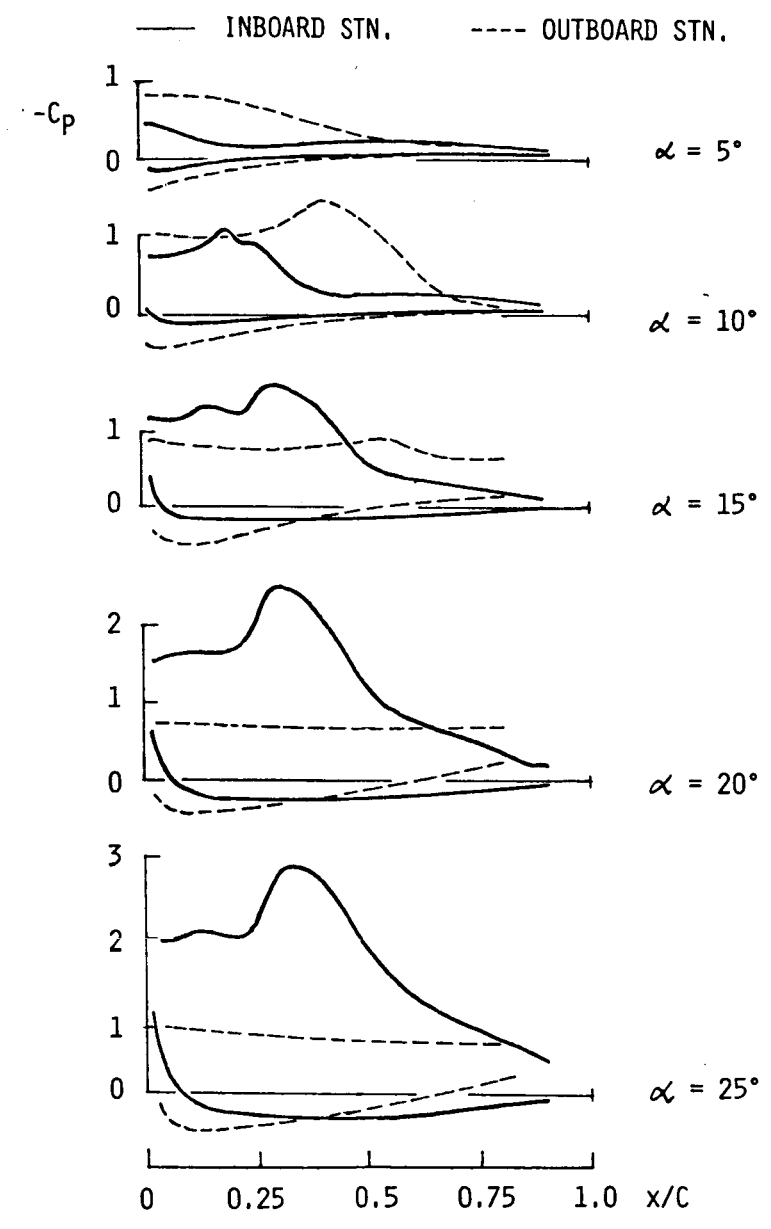


Figure 8 - Pressure distributions on basic cranked wing

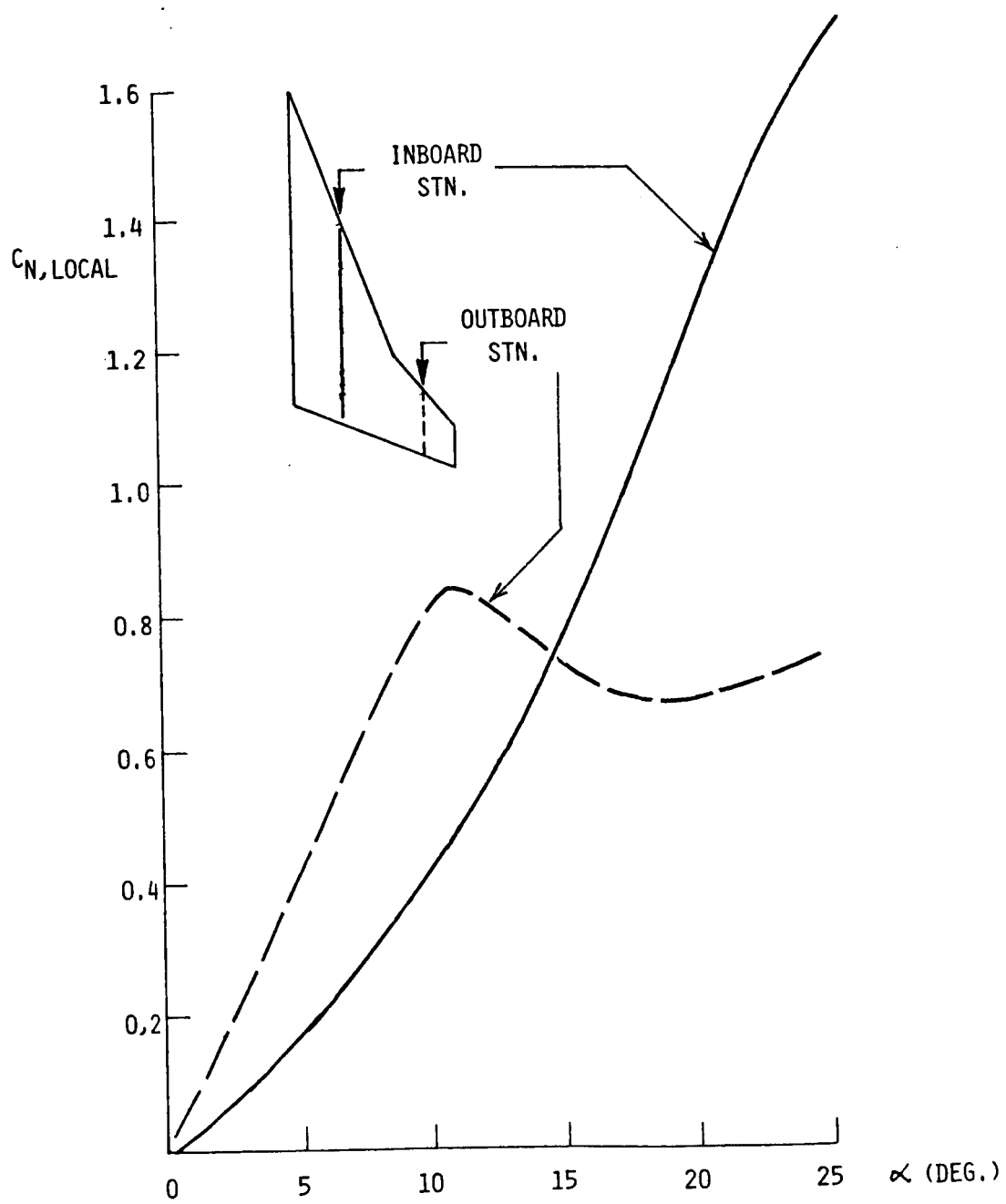


Figure 9 - Local normal force characteristics from integrated pressures on basic cranked wing.

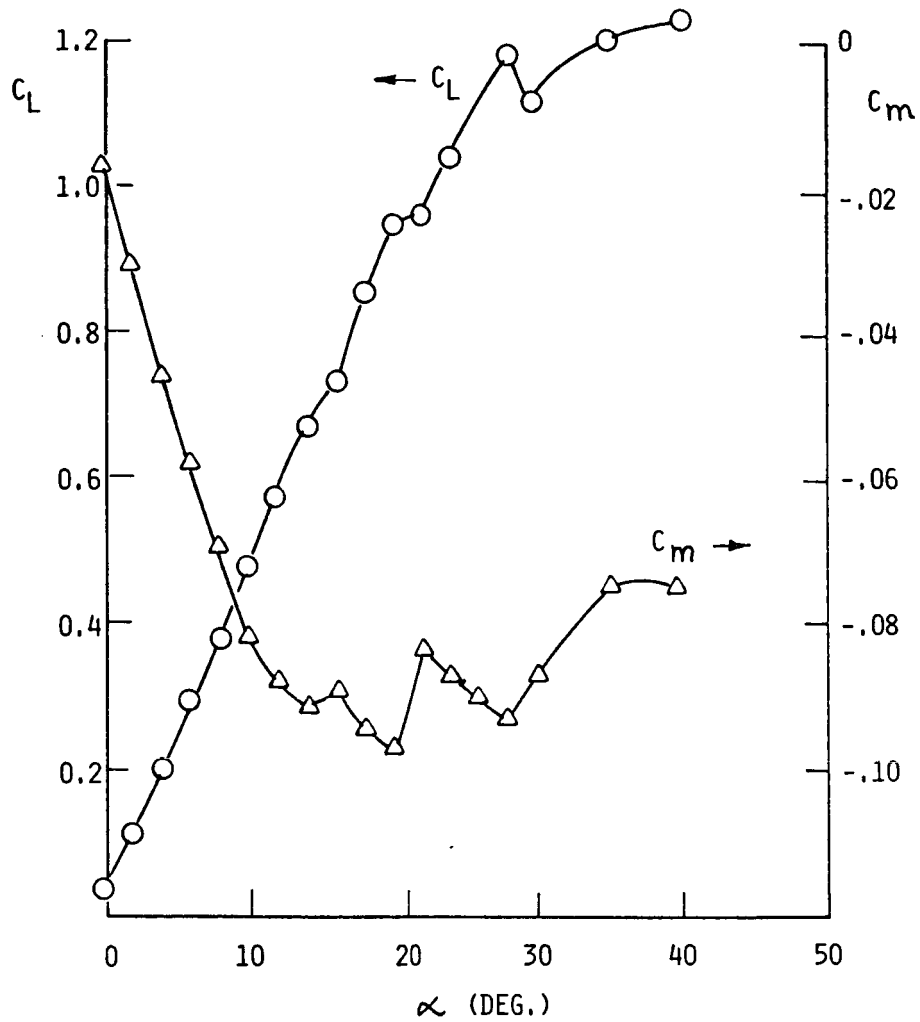
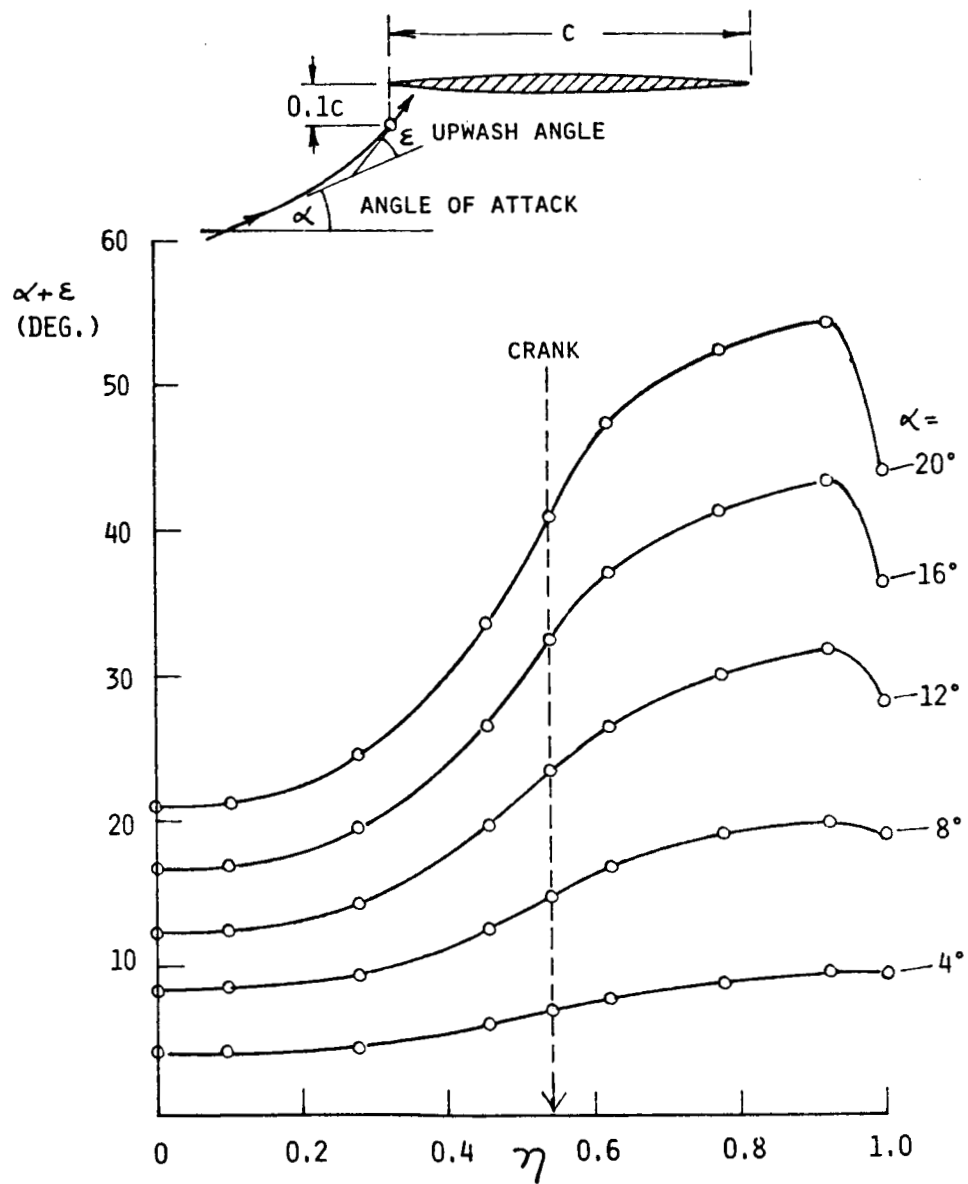
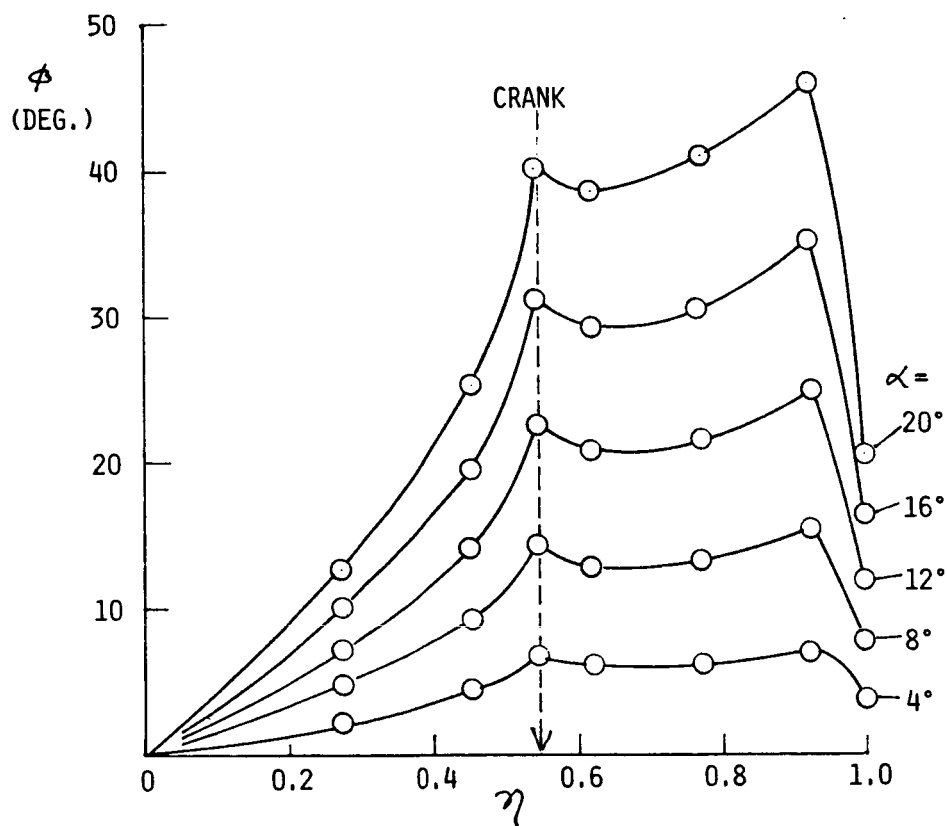


Figure 10 - Lift and pitching moment characteristics of basic cranked wing/body model.



A) Upwash

Figure 11 - Potential flow (PAN AIR) calculation of basic cranked wing



B) Sidewash

Figure 11 - Concluded

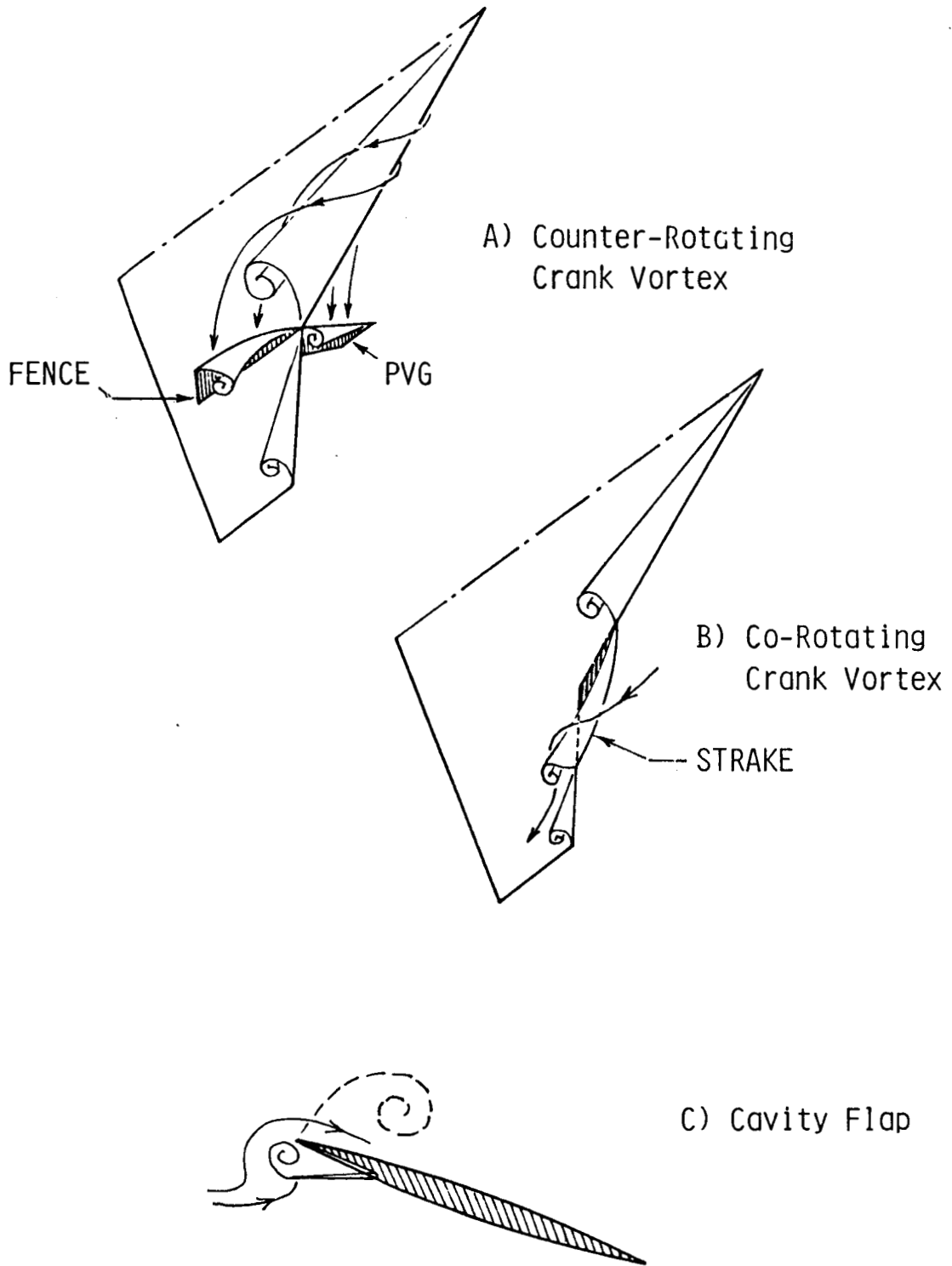


Figure 12 - Outboard panel flow control concepts

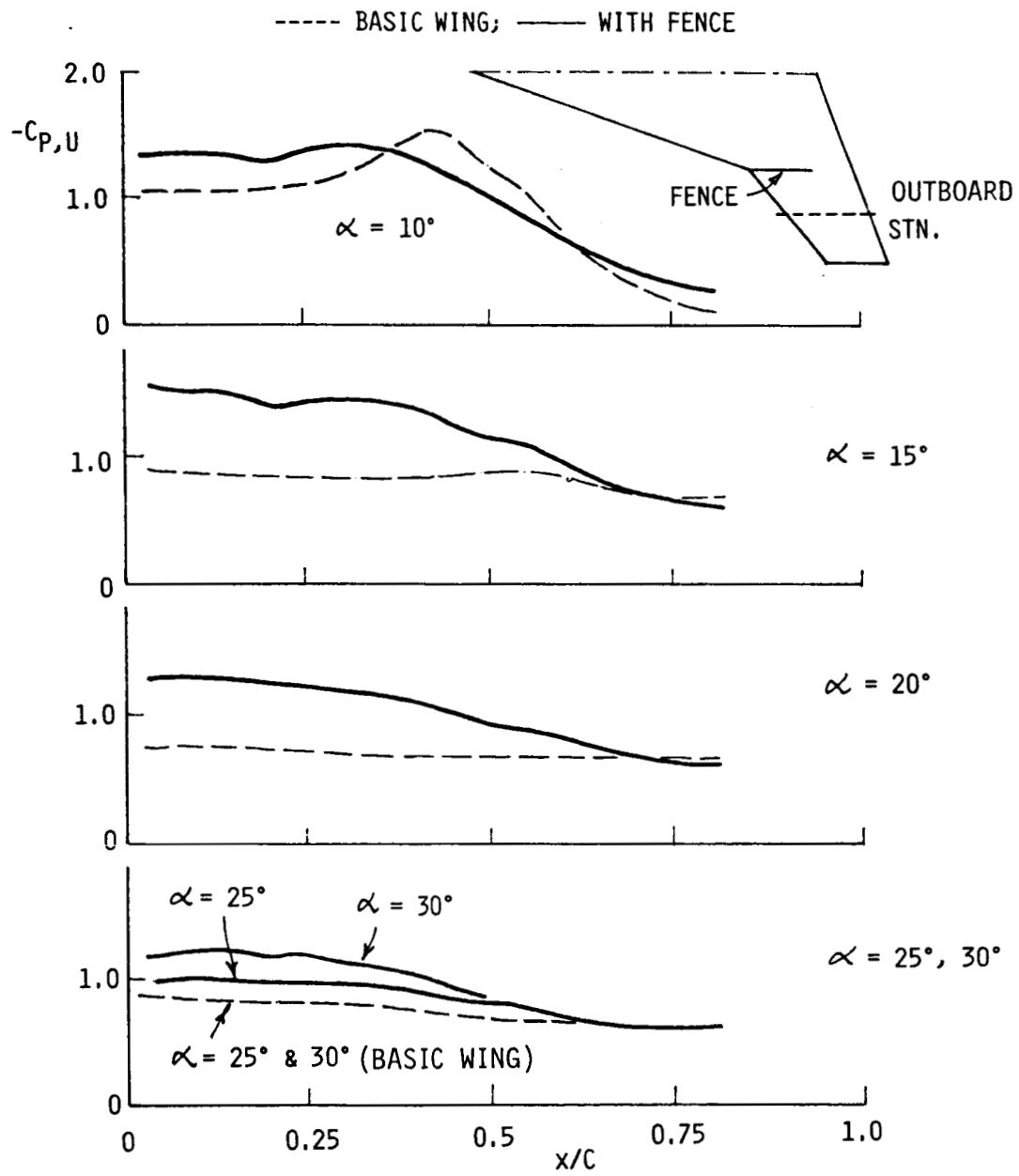


Figure 13 - Effect of fence on outboard panel upper-surface pressures

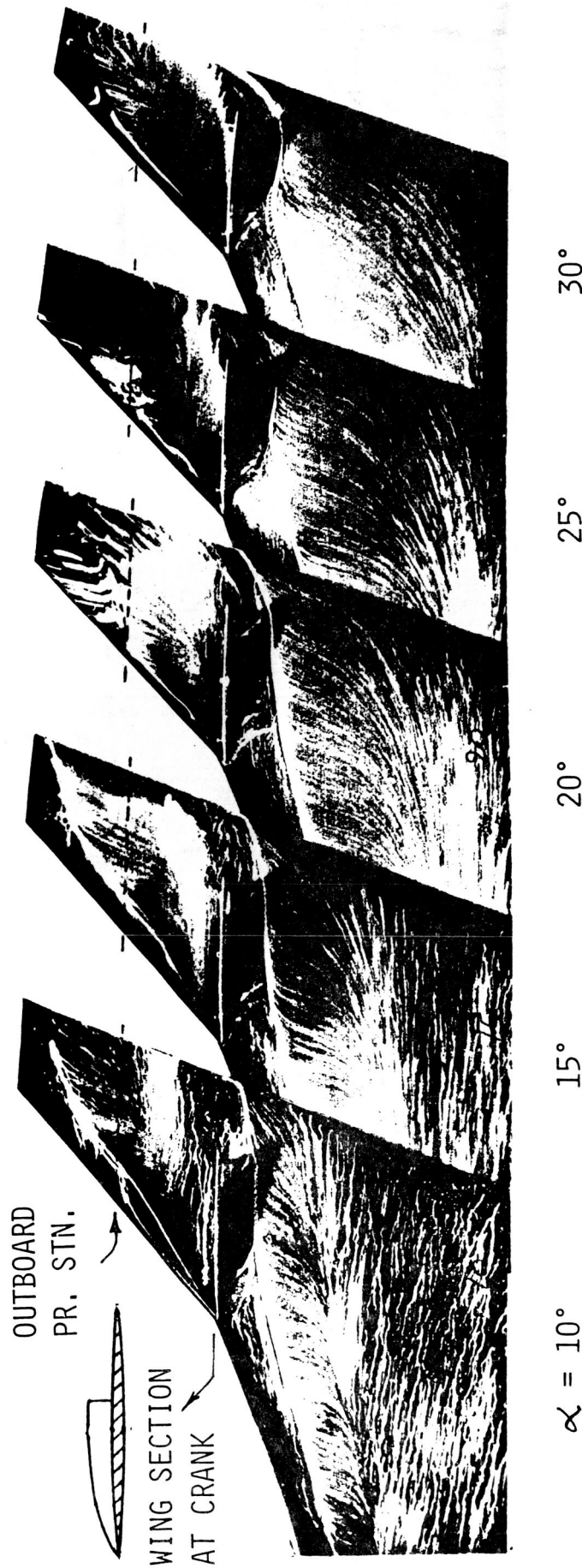


Figure 14 - Oil flow visualizations showing effect of fence on outboard panel flow development

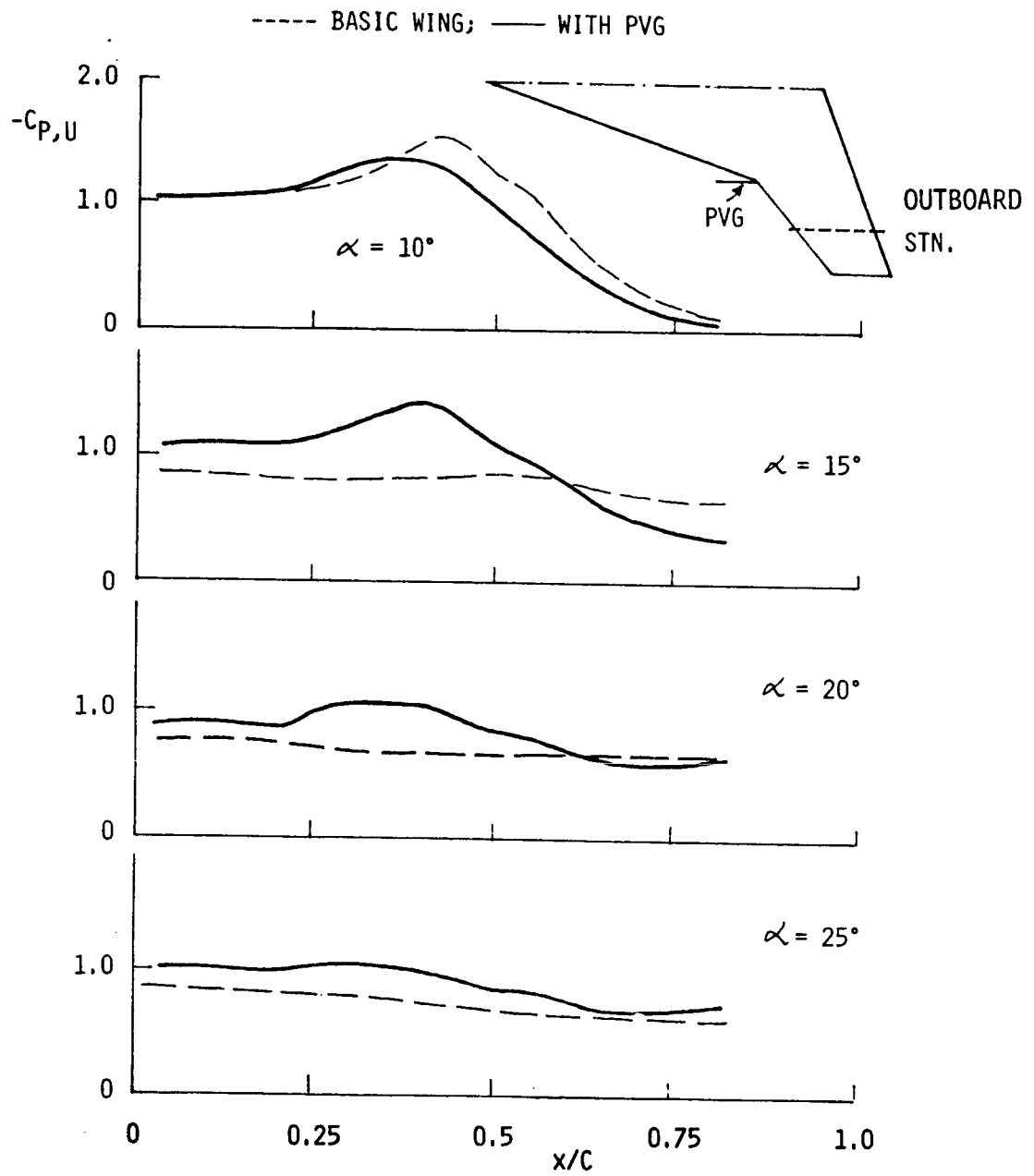


Figure 15 - Effect of PVG on outboard panel upper-surface pressures

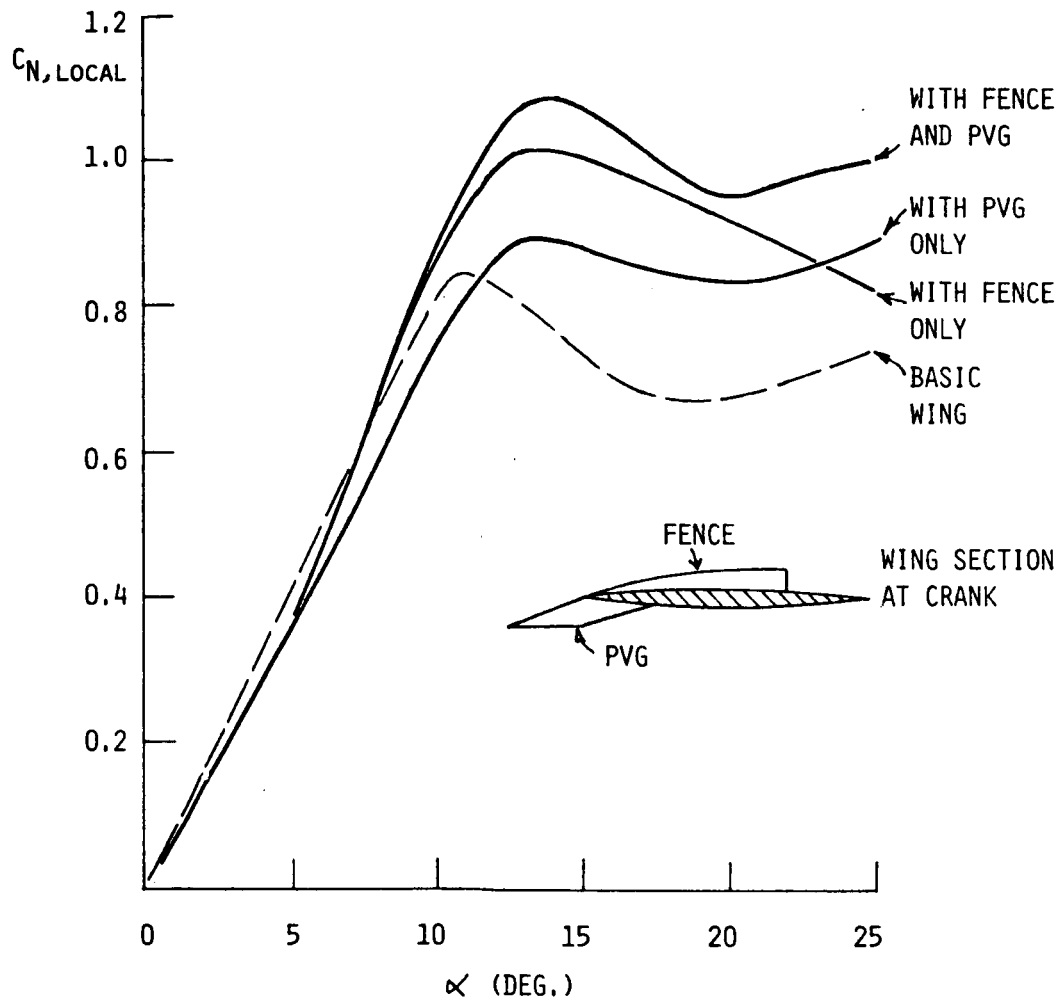


Figure 16 - Local normal force characteristics of outboard panel showing effect of devices

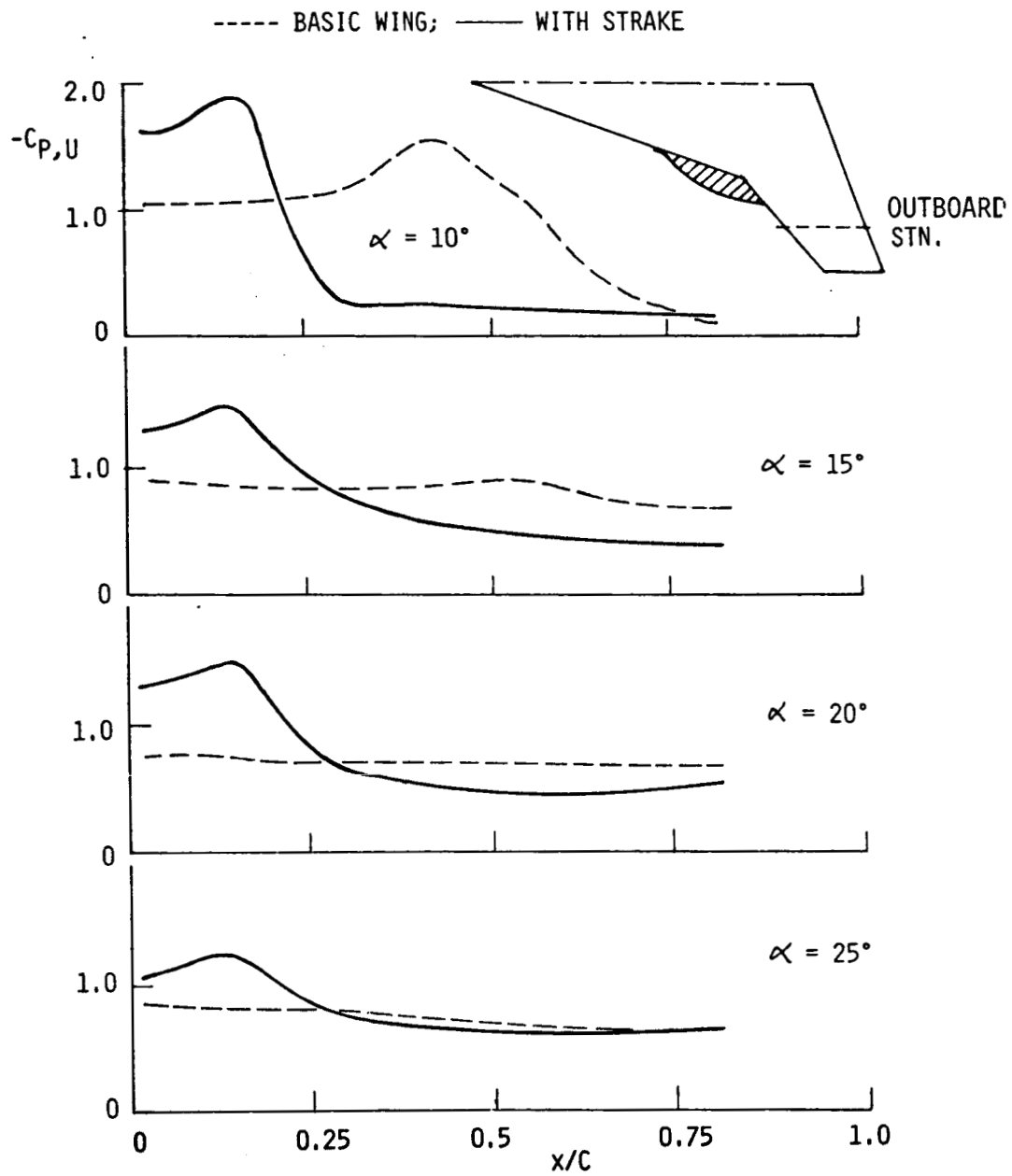


Figure 17 - Effect of folding strake on outboard panel upper-surface pressures

ORIGINAL PAGE IS
OF POOR QUALITY

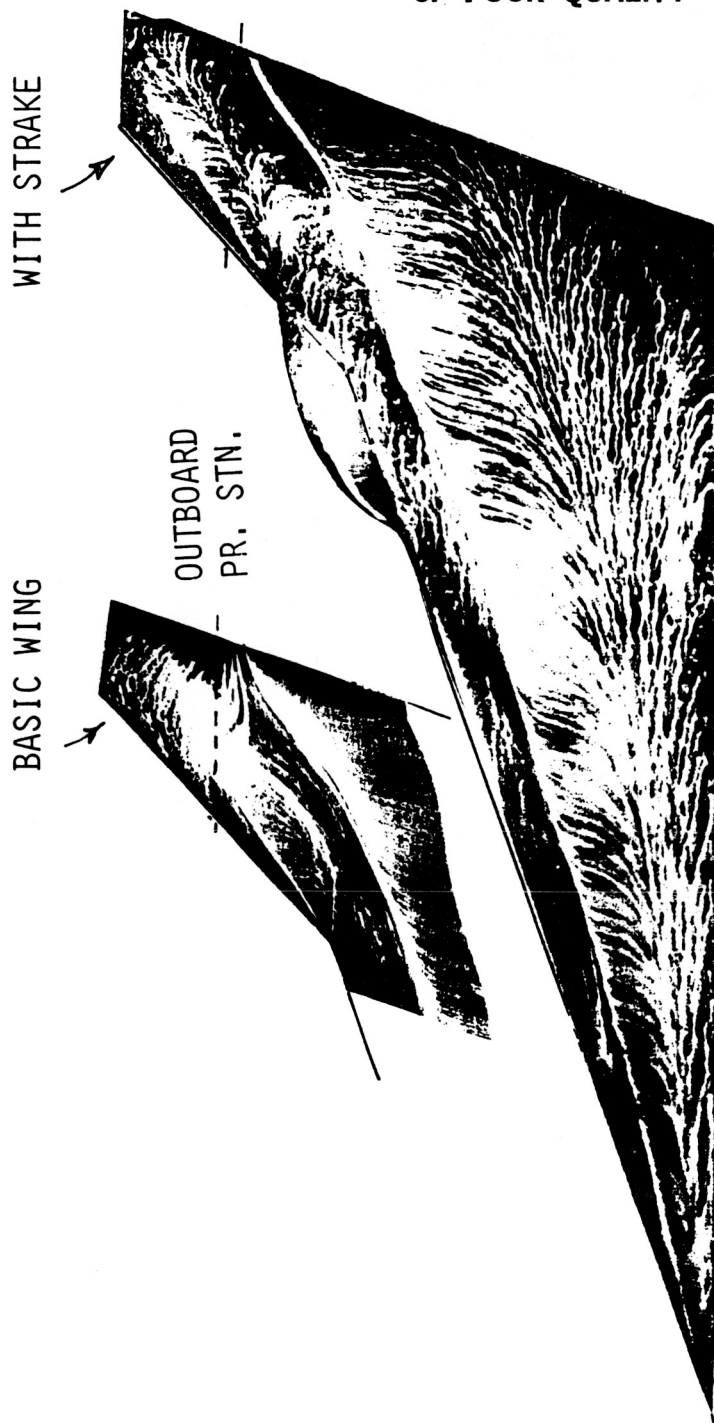


Figure 18 - Oil flow visualizations of wing and without folding strake at $\alpha = 20$ deg.

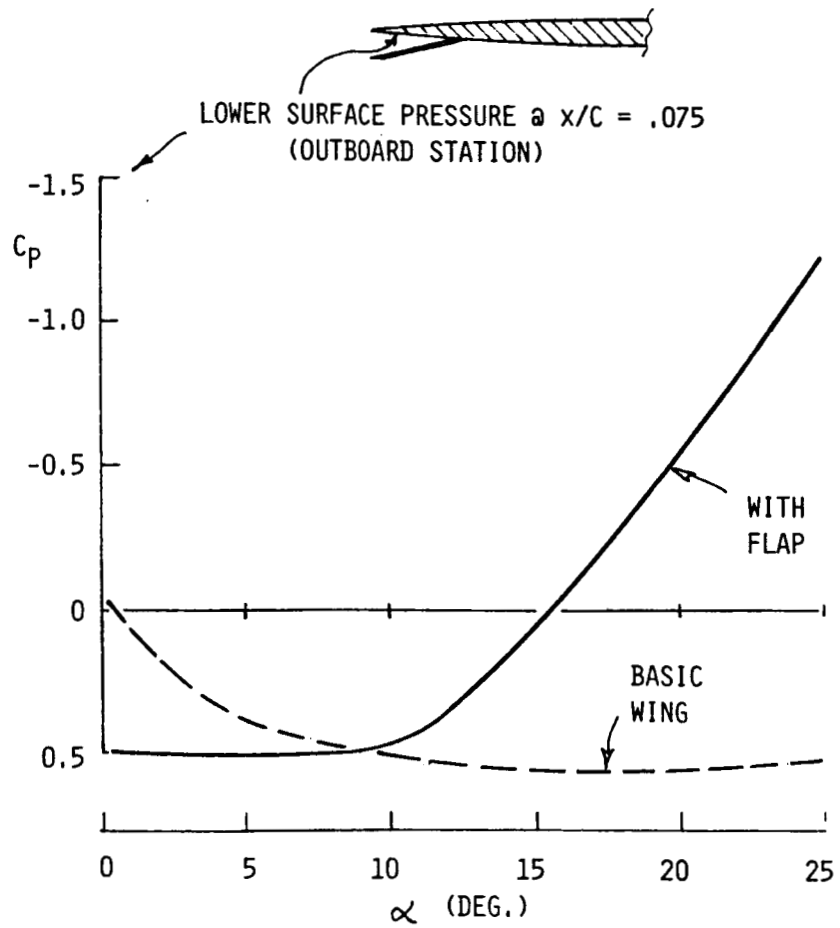


Figure 19 - Variation of cavity pressure with angle of attack, outboard cavity flap.

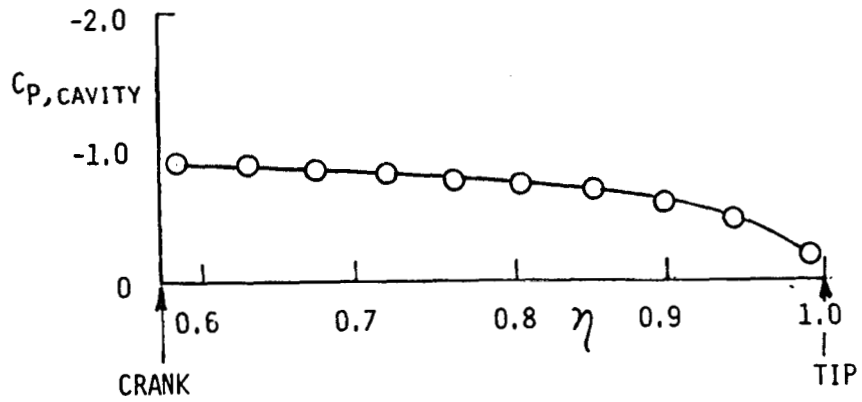


Figure 20 - Spanwise distribution of cavity pressure with outboard cavity flap at $\alpha = 25$ deg.

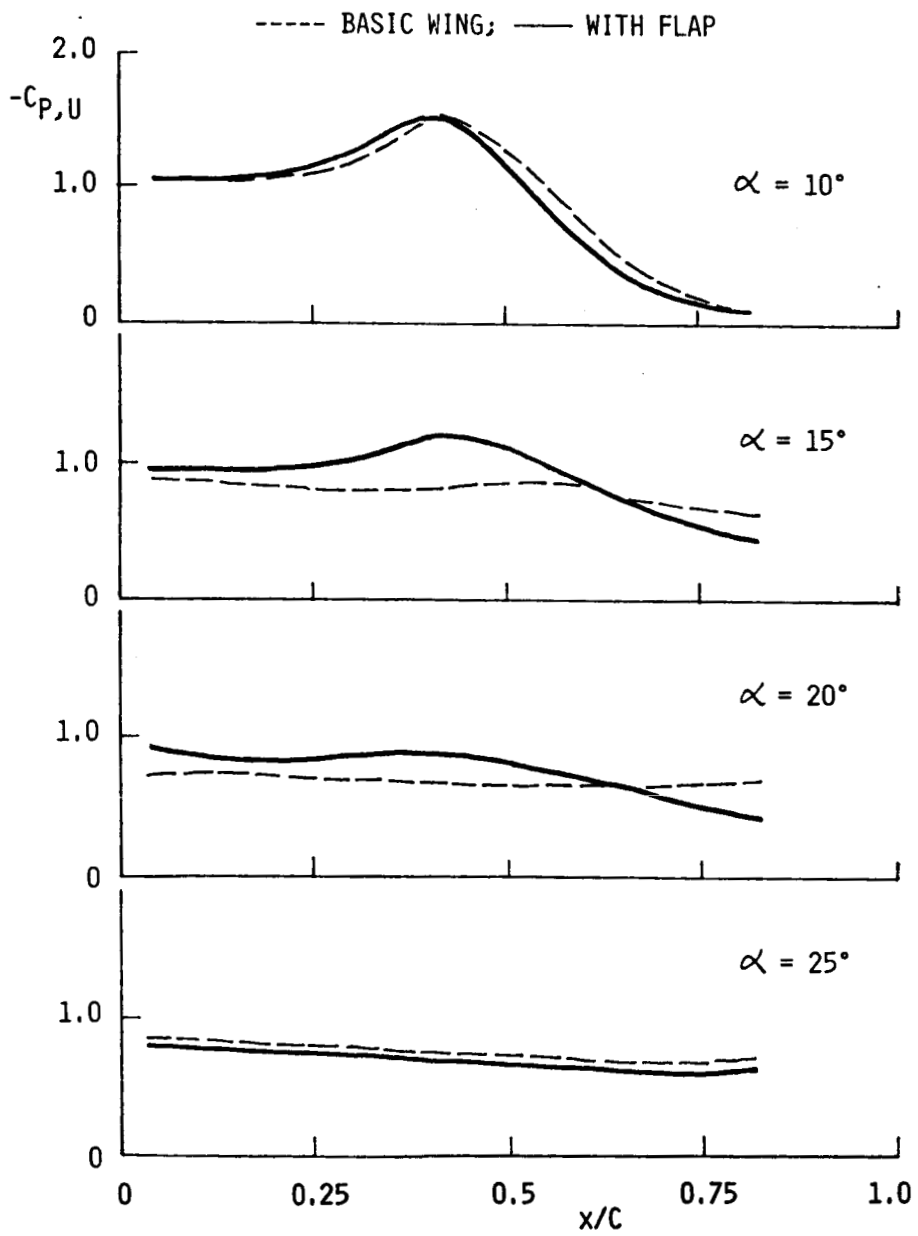


Figure 21 - Effect of outboard cavity flap on outboard panel upper-surface pressures

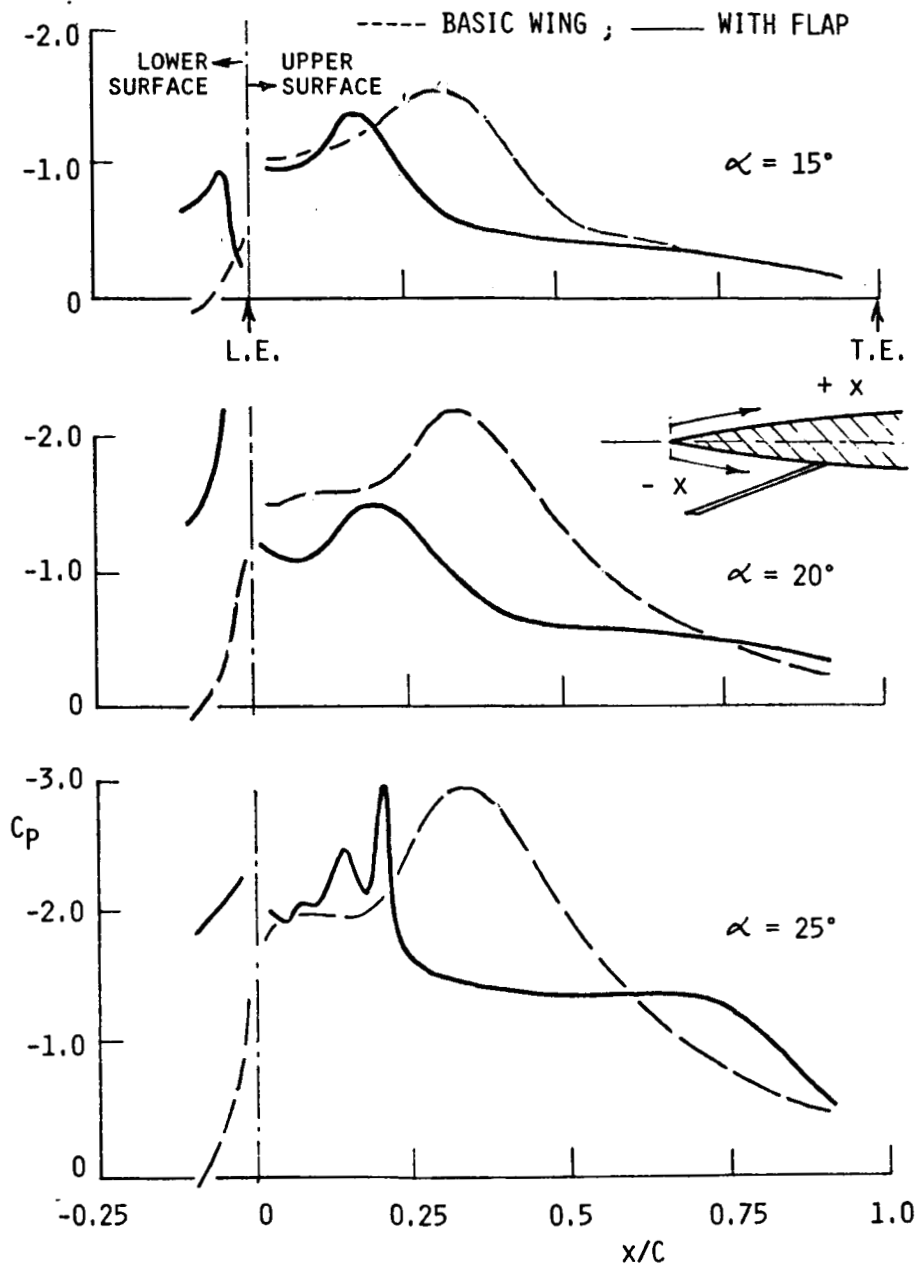


Figure 22 - Effect of inboard cavity flap on inboard panel upper-surface and cavity pressures

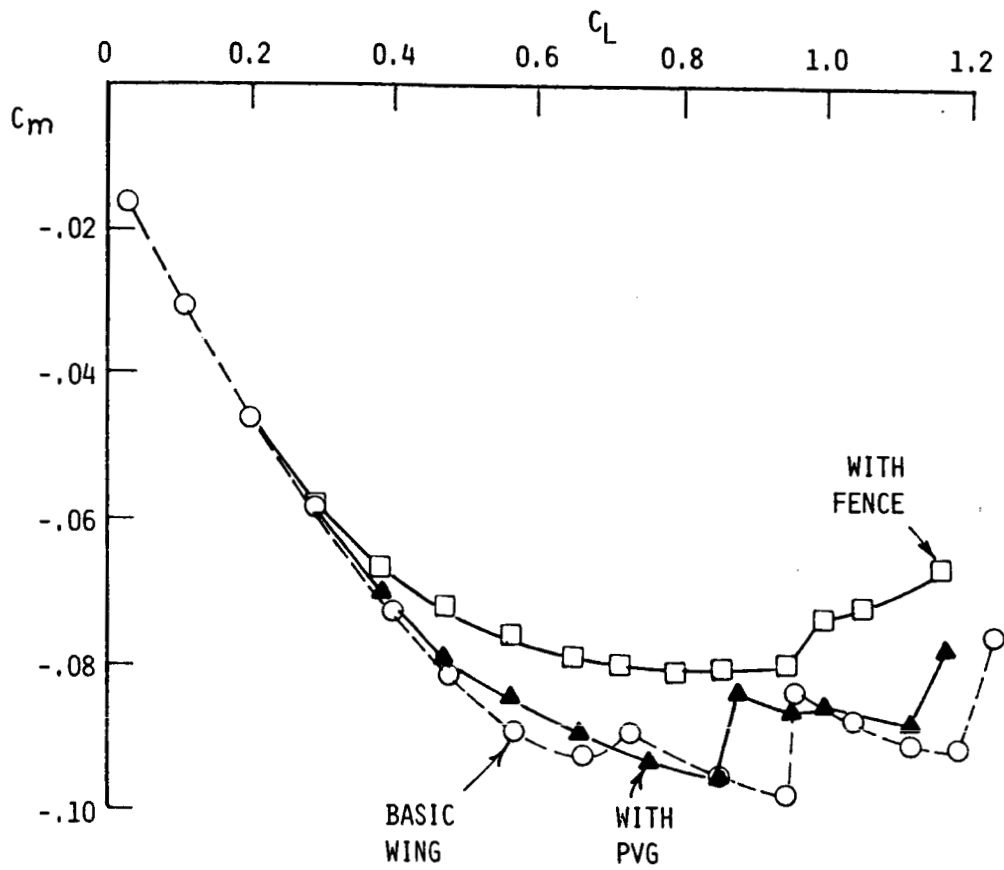


Figure 23 - Effect of fence and PVG on pitching moment characteristics of wing-body model.

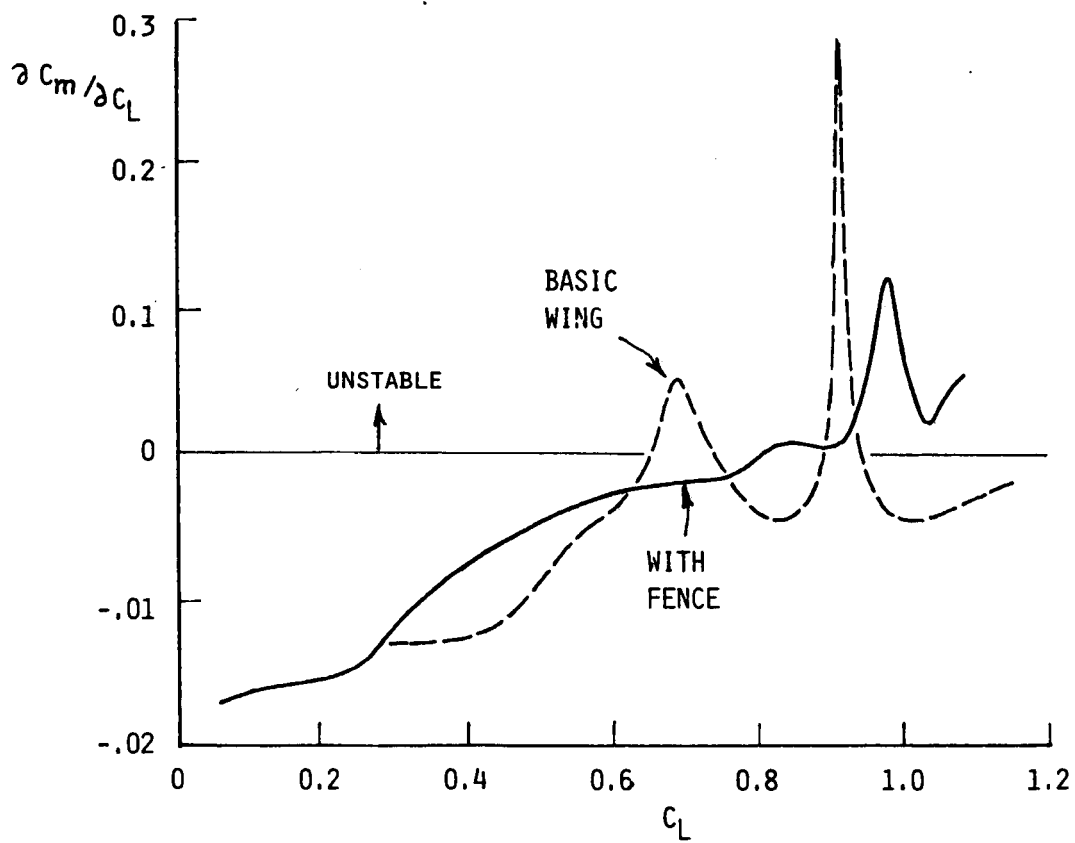


Figure 24 - Longitudinal stability derivative of wing-body model with and without fence

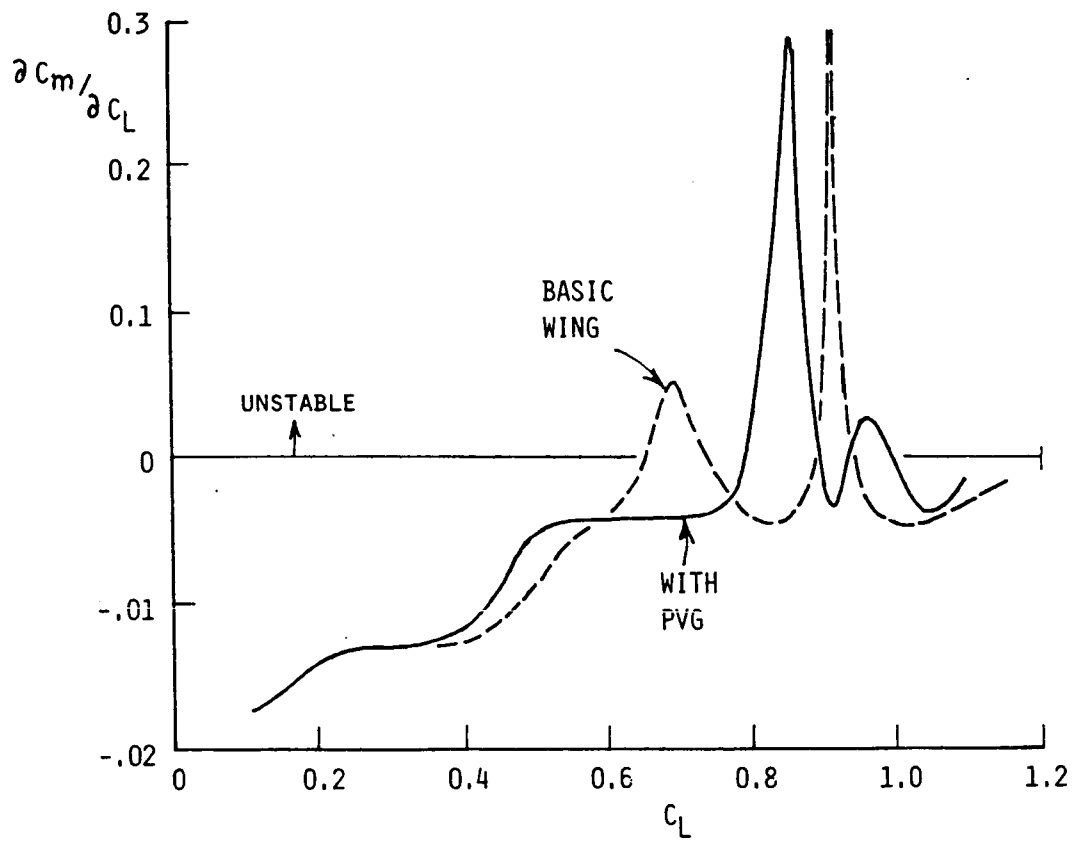


Figure 25 - Longitudinal stability derivative of wing-body model with and without PVG

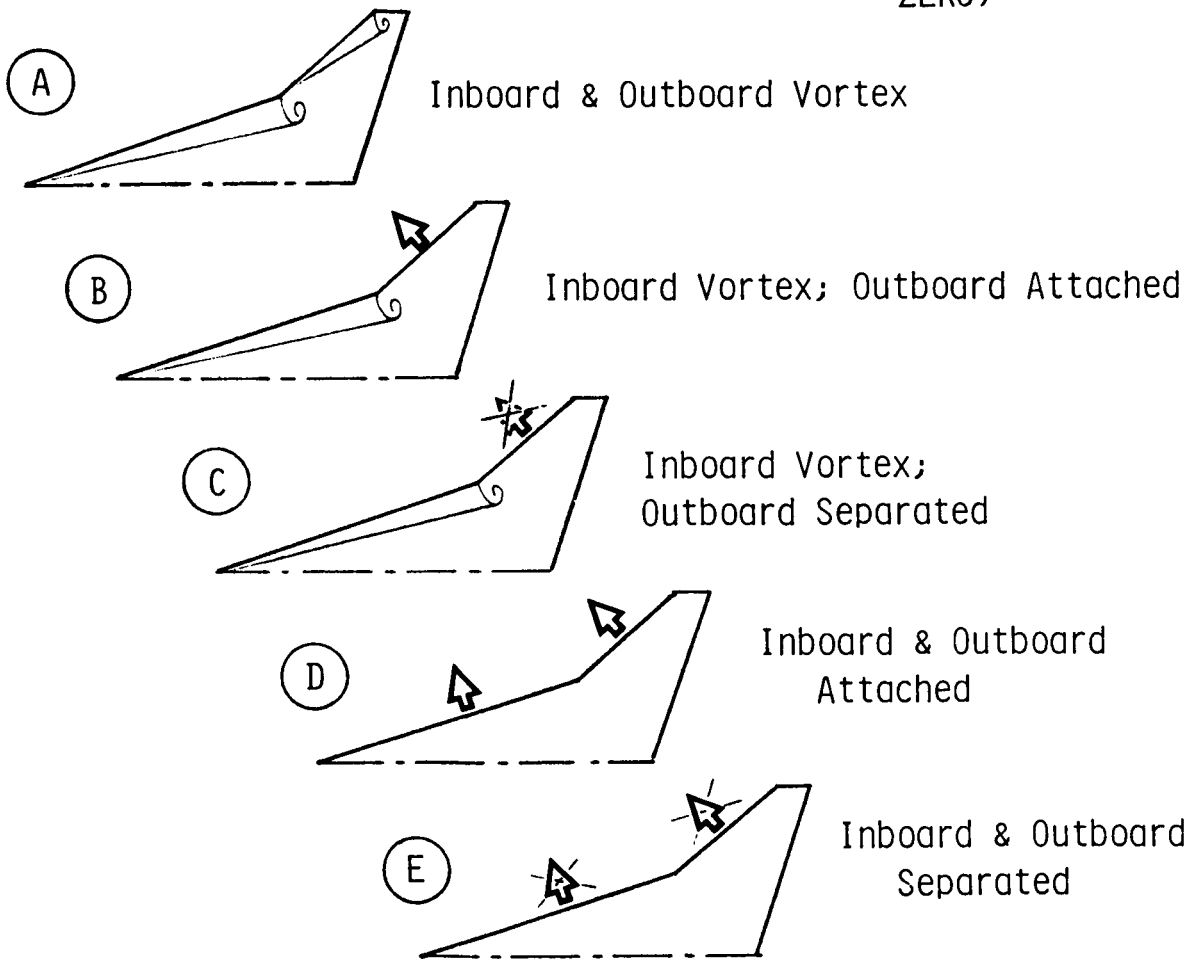
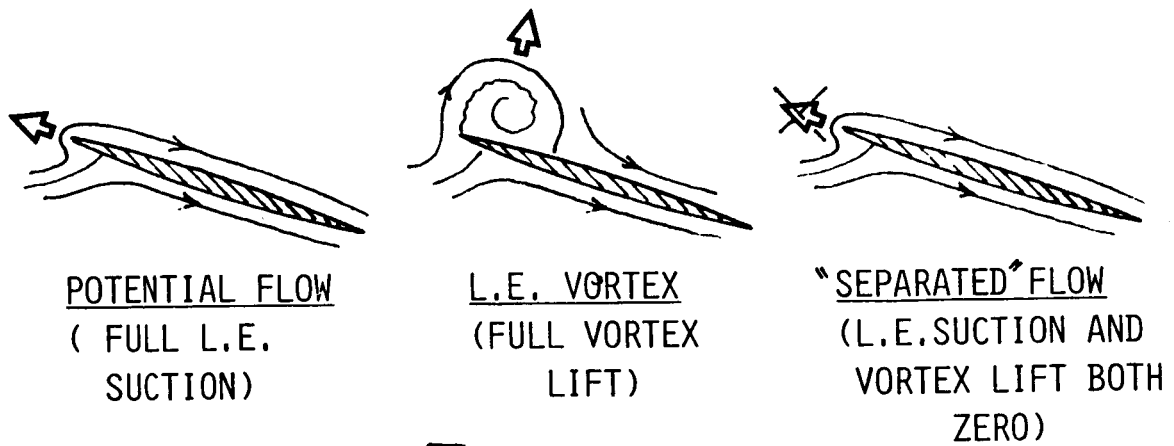


Figure 26 - Options in VLM-SA computation of basic wing

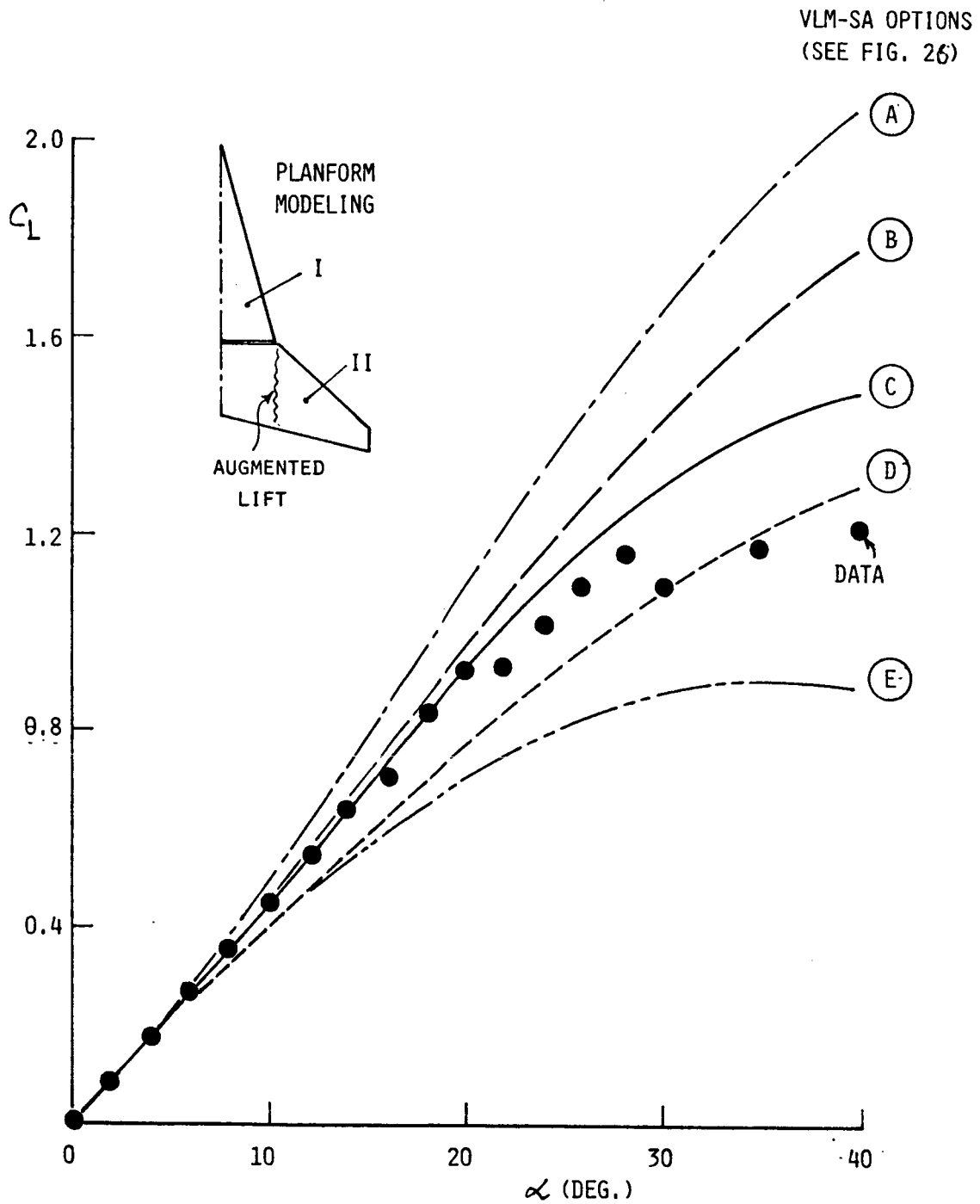


Figure 27 - Comparison of basic wing-body model lift data with various VLM-SA options (body not represented in VLM computation)

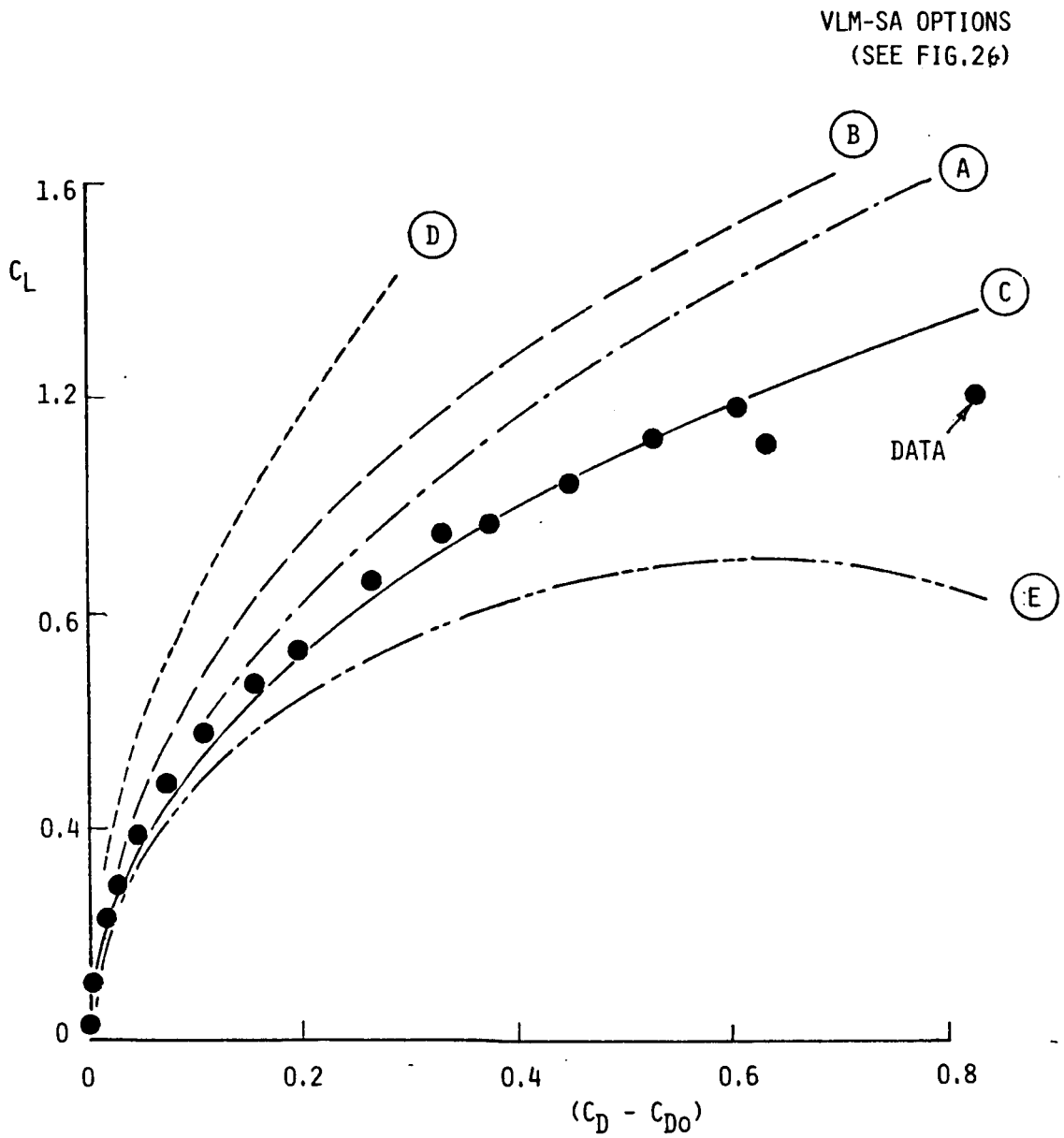


Figure 28 - Comparison of basic wing-body model drag polar with various VLM-SA options (body not represented in VLM computation)

Standard Bibliographic Page

1. Report No. NASA CR-178046		2. Government Accession No.		3. Recipient's Catalog No.	
4. Title and Subtitle SUBSONIC FLOW INVESTIGATIONS ON A CRANKED WING DESIGNED FOR HIGH MANEUVERABILITY				5. Report Date February 1986	
				6. Performing Organization Code	
7. Author(s) Dhanvada M. Rao				8. Performing Organization Report No.	
				10. Work Unit No.	
9. Performing Organization Name and Address Vigyan Research Associates, Inc. 28 Research Drive Hampton, VA 23666				11. Contract or Grant No. NAS1-17420	
				13. Type of Report and Period Covered Contractor Report	
12. Sponsoring Agency Name and Address National Aeronautics and Space Administration Washington, DC 20546				14. Sponsoring Agency Code 505-61-71-05	
				15. Supplementary Notes Langley Technical Monitor: William J. Small Final Report	
16. Abstract The characteristic pitching-moment nonlinearity of cranked wings limits their usable lift coefficient well below C_{Lmax} . The potential of several aerodynamic devices, viz. fences, pylon vortex generators (PVG), mid-span strakes and cavity flaps, in delaying the pitch-up onset on a 70/50 deg. cranked wing was explored in low-speed tunnel tests. Upper-surface pressure measurements and flow visualizations were conducted on a semi-span wing model to observe the vortex flow development with increasing angle of attack, and then to assess the effectiveness of the devices in controlling the collapse of vortex lift over the wing panel outboard of the crank. Force tests on a full-span wing and body model were also conducted to assess the fence and PVG in improving the usable C_L .					
17. Key Words (Suggested by Authors(s)) Pitch-Up Control Aerodynamic Devices Vortex Management Cranked Wing			18. Distribution Statement Unclassified-Unlimited Subject Category 02		
19. Security Classif.(of this report) Unclassified		20. Security Classif.(of this page) Unclassified		21. No. of Pages 44	22. Price A03

For sale by the National Technical Information Service, Springfield, Virginia 22161